AD-A047 825 ARMY ENGINEER TOPOGRAPHIC LABS FORT BELVOIR VA F/G 20/6
HOLOGRAPHIC OPTICAL ELEMENTS WITH LOW Q-FACTORS.(U)
OCT 77 W R GRAVER
UNCLASSIFIED ETL-0123 NL

1 OF 1
AD A047825

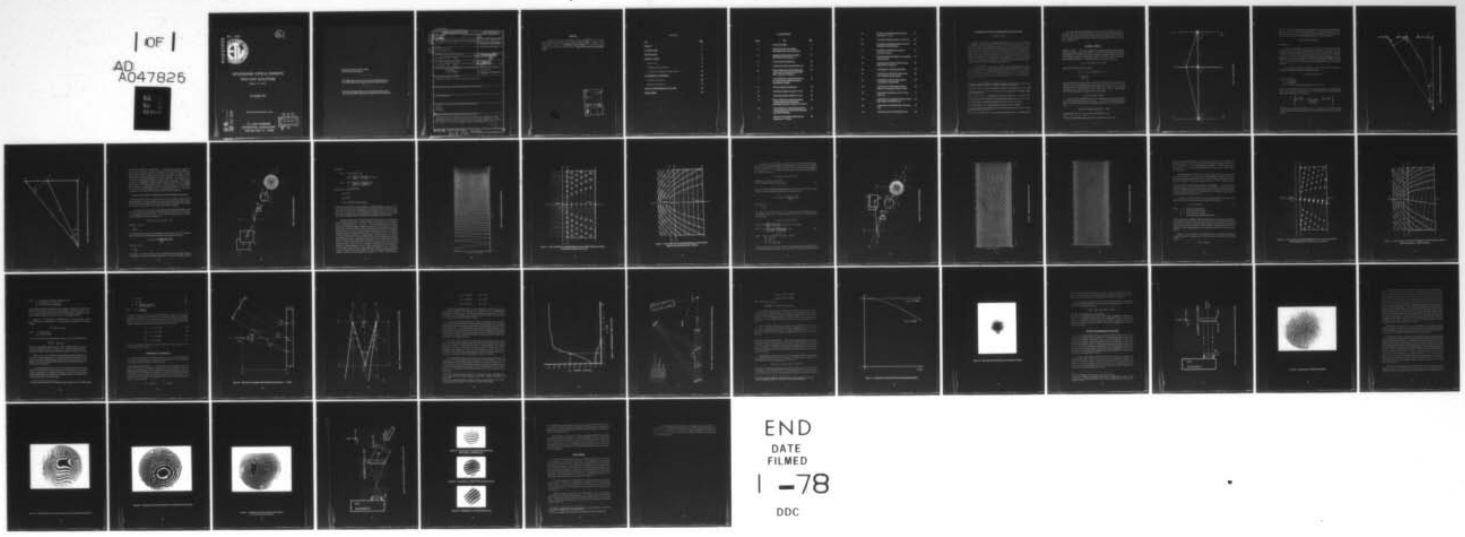

END
DATE FILMED
1-78
DDC

ETL - 0123

(12) SC

HOLOGRAPHIC OPTICAL ELEMENTS WITH LOW Q-FACTORS

William R. Graver

OCTOBER 1977

U.S. ARMY ENGINEER
TOPOGRAPHIC LABORATORIES
FORT BELVOIR, VA 22060

Destroy this report when no longer needed.
Do not return it to the originator.

The findings in this report are not to be construed as an official Department of the Army position unless so designated by other authorized documents.

The citation in this report of trade names of commercially available products does not constitute official endorsement or approval of the use of such products.

UNCLASSIFIED

SECURITY CLASSIFICATION OF THIS PAGE (When Data Entered)

REPORT DOCUMENTATION PAGE

READ INSTRUCTIONS BEFORE COMPLETING FORM

1. REPORT NUMBER: ETL-0123
2. GOVT ACCESSION NO.:
3. RECIPIENT'S CATALOG NUMBER:
4. TITLE (and Subtitle): HOLOGRAPHIC OPTICAL ELEMENTS WITH LOW Q-FACTORS.
5. TYPE OF REPORT & PERIOD COVERED: Research Note 1975-1976
6. PERFORMING ORG. REPORT NUMBER:
7. AUTHOR(s): William R. Graver
8. CONTRACT OR GRANT NUMBER(s):
9. PERFORMING ORGANIZATION NAME AND ADDRESS: U.S. Army Engineer Topographic Laboratories, Fort Belvoir, Va. 22060
10. PROGRAM ELEMENT, PROJECT, TASK AREA & WORK UNIT NUMBERS: 4A161102B52C-05-0001
11. CONTROLLING OFFICE NAME AND ADDRESS: U.S. Army Engineer Topographic Laboratories, Fort Belvoir, Va. 22060
12. REPORT DATE: October 1977
13. NUMBER OF PAGES: 44
14. MONITORING AGENCY NAME & ADDRESS (if different from Controlling Office): 46p.
15. SECURITY CLASS. (of this report): Unclassified
15a. DECLASSIFICATION/DOWNGRADING SCHEDULE:
16. DISTRIBUTION STATEMENT (of this Report): Approved for public release; distribution unlimited
17. DISTRIBUTION STATEMENT (of the abstract entered in Block 20, if different from Report):
18. SUPPLEMENTARY NOTES:
19. KEY WORDS (Continue on reverse side if necessary and identify by block number):
Optics
Lasers
Holography
20. ABSTRACT (Continue on reverse side if necessary and identify by block number):

Holographic optical elements, with low Q-factors, are theoretically modeled and experimentally constructed. An optical performance evaluation yields (1) a low reconstruction angle sensitivity of 14 degrees, (2) a high diffraction efficiency of 50 percent, and (3) an optical path deviation of $\lambda/4$.

DD FORM 1 JAN 73 1473 EDITION OF 1 NOV 65 IS OBSOLETE

UNCLASSIFIED

SECURITY CLASSIFICATION OF THIS PAGE (When Data Entered)

403 192

PREFACE

Experimental research in Holographic Optical Elements with Low Q-factors was performed under Project Number 4A161102B52C-05-0001, "Research in Coherent Optics," Work Unit: ***Holographic Optical Elements.*** The optical performance evaluation was performed under Work Unit: ***Optical Mass Memories Using Coherent Optics***.

CONTENTS

ILLUSTRATIONS

HOLOGRAPHIC OPTICAL ELEMENTS WITH LOW Q-FACTORS

INTRODUCTION

Research in holographic optical elements (HOE) stems from previous studies in holographic correction plates (HCP).[1,2,3] There are two similarities between the HOE and HCP; (1) both record patterns generated by two interfering wavefronts of laser light, and (2) both produce perfect point-imaging when reilluminated with laser light. However, the HOE and HCP are dissimilar in two respects; (1) the HCP performs as a phase corrector that optimizes a conventional lens, whereas the HOE performs as an optimized conventional lens for coherent light, and (2) the HCP is restricted to imaging conditions imposed by its complementary lens, whereas the HOE itself has focal power. Thus, the HOE has more versatility in satisfying the functional requirements of coherent optical information processing systems than the HCP.

Former work[4,5,6,7] with holographic optical elements stressed Bragg diffraction effects in volume[8] holograms where the Q-factor[9] was greater than 10. Since a hologram with a high Q-factor ($Q > 10$) exhibits maximum first-order diffraction intensity and a very low Q-factor hologram ($Q < 1$) exhibits maximum latitude of reconstruction angle, it is reasonable to expect both properties combined in a low Q-factor hologram bounded by $1 < Q < 10$.

---

1 W.R. Graver, *Holographic Compensation of Wavefront Aberrations in Optical Systems*, U.S. Army Engineer Topographic Laboratories, Fort Belvoir, Va., ETL-RN-74-11, June 1975, NTIS: AD-A013 978.

2 J.E. Ward, D.C. Auth, and F.P. Carlson, "Holographically Generated Lens," *Applied Optics*, Vol. 10, 1971, p. 896.

3 J. Upatnieks, A. Vander Lugt, and E. Leith, "Correction of Lens Aberrations by Means of Holograms," *Applied Optics*, Vol. 5, 1966, p. 589.

4 A.K. Richter and F.P. Carlson, "Holographically Generated Lenses," *Applied Optics*, Vol. 13, 1974, p. 2924.

5 J.D. Hovis, *The Production and Evaluation of Dichromated Holographic Lenses*, March 1974, NTIS: AD-777-845.

6 R.C. Seid, *The Production and Evaluation of Holographic Lenses*, June 1973, NTIS: AD-764-701.

7 R.G. Zech, *Investigation of Uses of Holographic Optical Elements*, May 1973, NTIS: N73-28555.

8 F.G. Kaspar, "Diffraction by Thick, Periodically Stratified Gratings with Complex Dielectric Constant," *J. Optical Society of America*, Vol. 63, 1973, p. 37.

9 H. Kogelnik, "Coupled Wave Theory for Thick Hologram Gratings," *Bell System Tech. J.*, Vol. 48, 1969, p. 2909.

This report describes investigations of the virtues of a low Q-factor HOE. The investigation was to accomplish the following: (1) computer modeling and subsequent physical construction of a HOE with different reference-to-subject intensity ratios, and (2) a comparison between a low Q-factor HOE and a standard glass lens using interferometric measurements.

GENERAL THEORY

FRESNEL ZONES. The general properties of holographic optical elements are best understood through Fresnel zone construction as originally described by the Huygen-Fresnel theory.[10] The Fresnel zone model consists of a monochromatic point source P, illuminating the plane U, V as observed from the point P'. From figure 1, we can express the total optical path r + r' through any point u, v in the U, V plane as:

$$(r + r') = (h^2 + R^2)^{1/2} + (h'^2 + R^2)^{1/2}$$

Applying the binomial expansion, we get

$$(r + r' = h + h' + \tfrac{1}{2} R^2 (1/h + 1/h') + \cdots$$

for $R^4 < h^4$
$R^4 < h'^4$

Now, consider the loci of points in the U, V plane for only those discrete values of R as defined by each one-half wavelength increment in (r + r') for all (r + r') > (h + h'). The resulting concentric regions bounded by the circular loci are called Fresnel zones and are defined by $R_n = \sqrt{n\lambda L}$ where $L = (1/h + 1/h')^{-1}$ for n = 1,2,3, . . . regions. Note that all Fresnel zones are of equal area, since for any n value,

$$\pi(R_n)^2 - \pi(R_{n-1})^2 = \pi R^2_1.$$

The total optical disturbance at P' can be expressed in terms of the sum of contributions of each Fresnel zone, W_1, W_2, W_3 . . ., in which the average phase of the light incident at each zone differs by π between adjacent zones. Thus, the total amplitude

$$|W_{p'}| = |W_1| - |W_2| + |W_3| - |W_4| + \cdots |W_n|$$

would be nearly zero if n is even or approximately $|W_1|$ if n is odd.

---

[10] M. Born and E. Wolf, *Principles of Optics*, (5th Ed.), New York: Pergamon Press, 1975, P. 370.

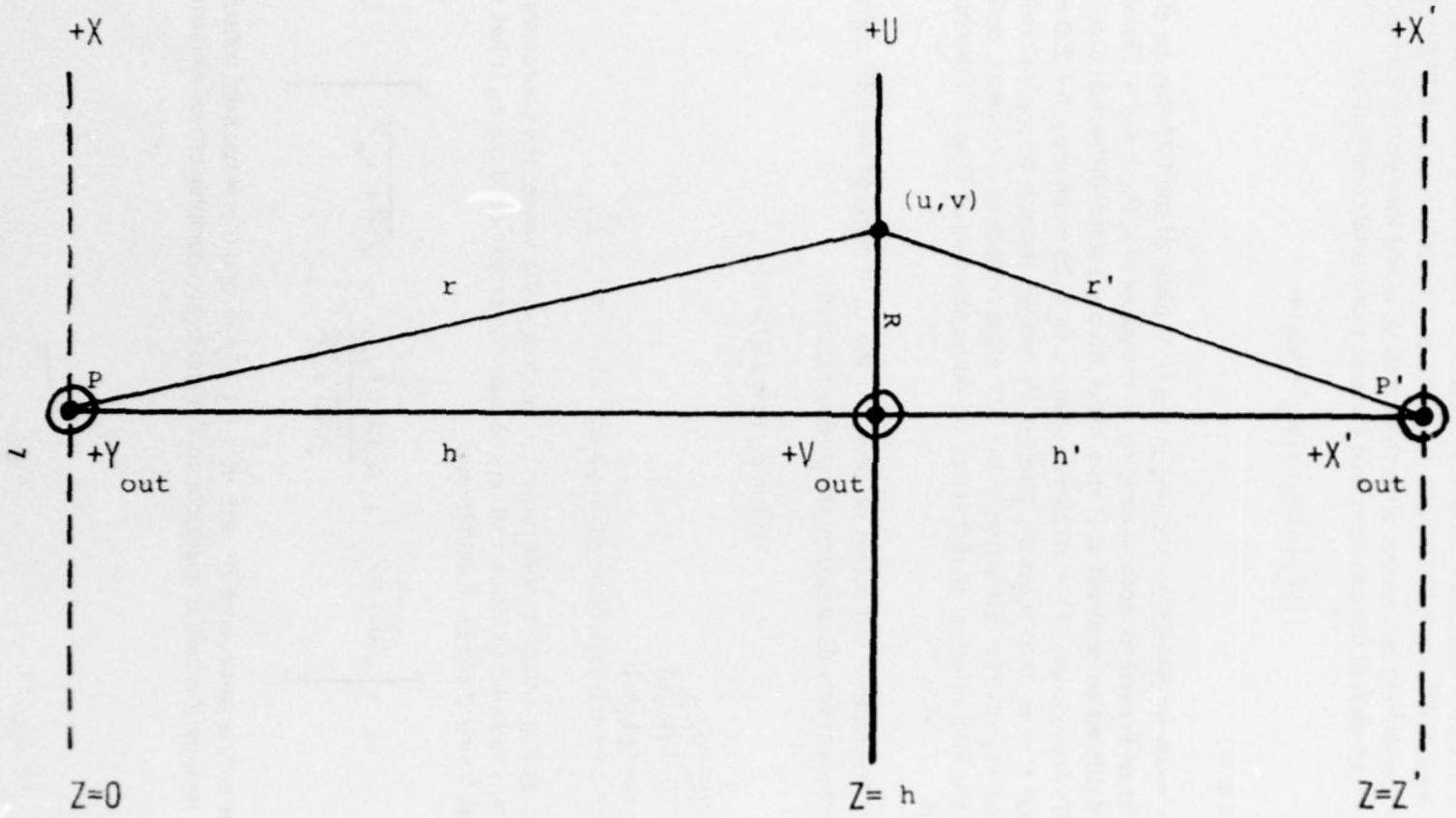

Figure 1. Fresnel Zone Model

However, if the even numbered zones are obstructed, the resulting zones would then constitute a series of concentric annular apertures or a Fresnel zone plate (FZP). This zone plate, performing as a special diffraction grating, would then scatter the incident wavefronts from each of the odd-numbered zones so that a total contribution

$$|W_{p'}| = |W_1| + |W_3| + |W_5| + \cdots$$

is observed at P'.

The mode of diffraction occuring in the U, V plane of the FZP may be either Fraunhoffer or Fresnel, or both, depending on the values of λ, R_n, h and h'. However, the general diffraction observed at P' may differ from the actual diffraction occurring in the FZP. For example, if λ = .6328 micrometers, $R_n \cong 25$ millimeters, h = 200 millimeters, and h' = ∞, then zones W_1 through W_7 and W_7 through W_{4938} will exhibit Fresnel and Fraunhoffer diffraction in the FZP plane respectively. However, because h' = ∞, the total effect of all diffraction would be observed at P' as a Fraunhoffer diffraction.

The Fraunhoffer diffraction occurring in the U, V plane of the FZP owing to P may be conveniently described by the grating equation

$$d\,(\sin\theta_n + \sin\theta'_n) = m\lambda$$

where $d = R_n - R_{n-2}$

$\theta_n = \tan^{-1}(R_n/h)$

$\theta'_n = \tan^{-1}(R_n/h')$

m = + 1 for this case, although in general m = 0, ± 1, ± 2, ...

Since the grating equation holds only for incident plane waves, the approximation $\theta_n \sim \theta_{n-2}$ is required to insure that any $\Delta\lambda$ over the projection $d \cos\theta_n$ is less than 1/10 λ (see figures 2 and 3). A definition is

$$\Delta\lambda = \left[\sqrt{h^2 + R_{n-2}^2} + \frac{R_n(R_n - R_{n-2})}{\sqrt{h^2 + R_n^2}} - \sqrt{h^2 + R_n^2} \right]$$

Note that only a particular FZP with m = + 1, r' = ∞, and h' = ∞ has been considered in detail because this case is analogous to the ensuing holographic optical element discussion.

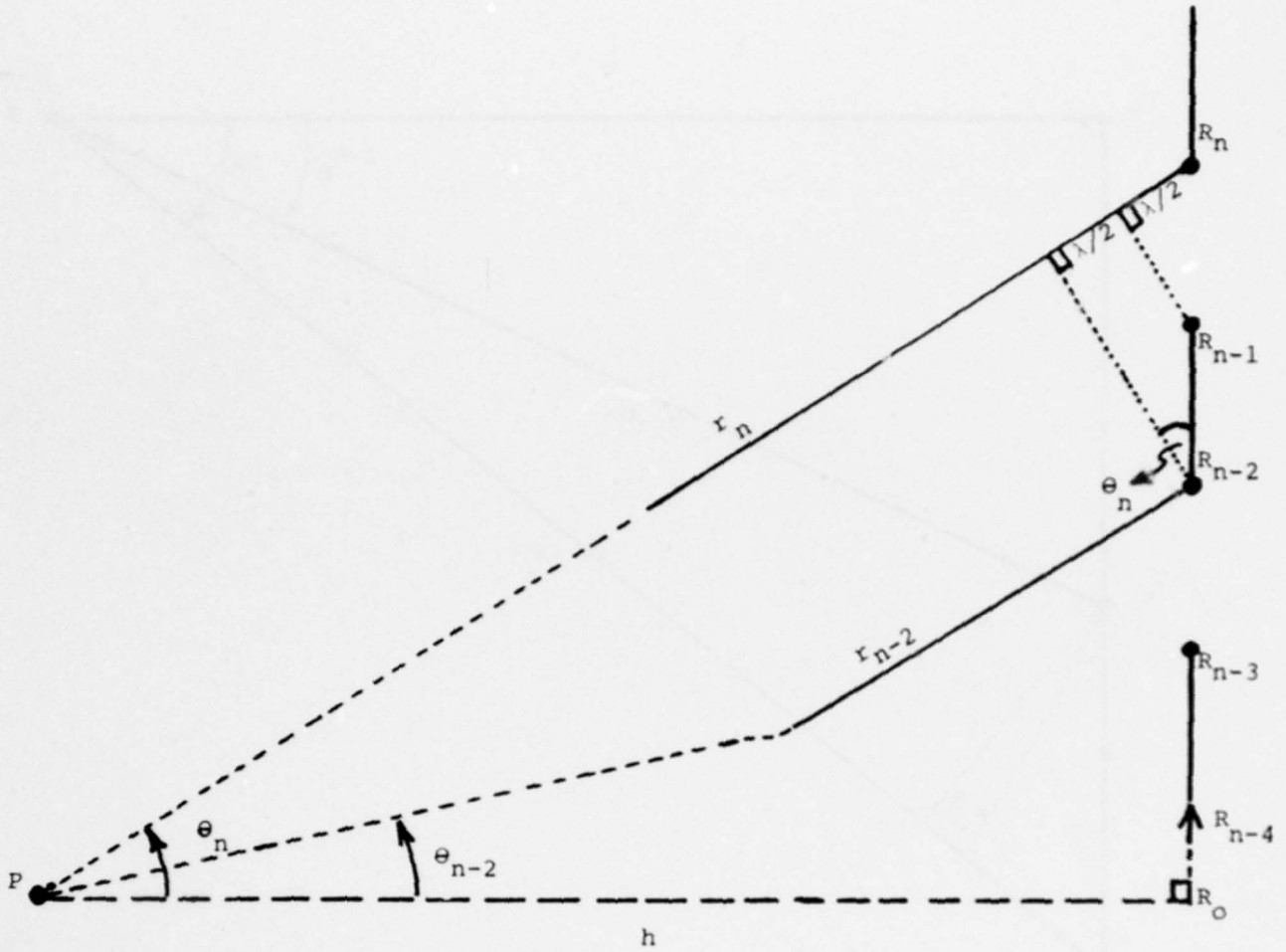

Figure 2. Phase Differences in the Incident Plane Waves at the Fresnel Zone Plate.

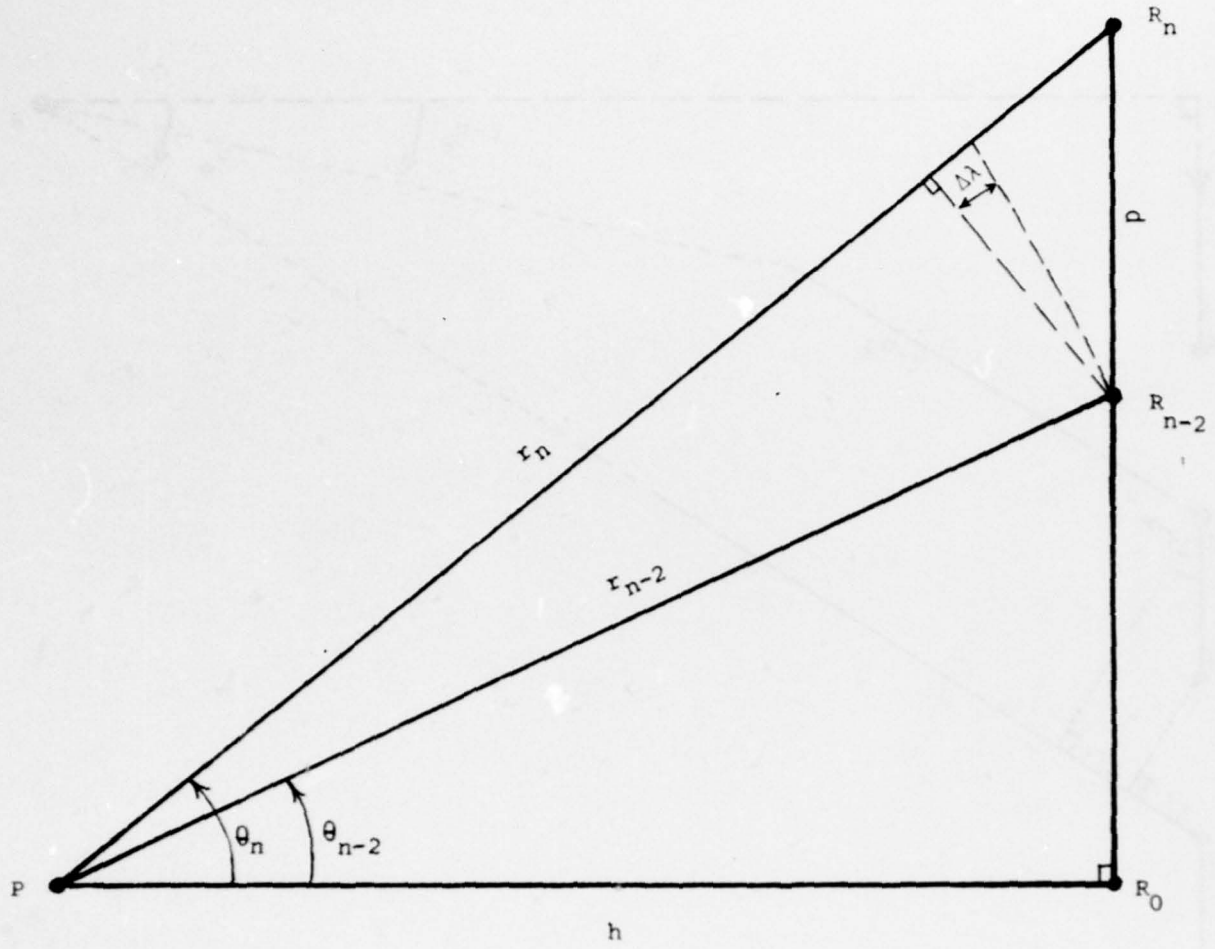

Figure 3. Applying the Grating Equation Within the Optical Path Limitation ($\Delta\lambda$).

HOLOGRAPHIC OPTICAL ELEMENTS. A holographic optical element (HOE) is a special type of hologram. An HOE is formed by recording the interference pattern between diverging spherical waves and plane waves. The medium of record is usually photosensitive, and the recorded pattern is called a hologram. If the HOE is re-illuminated by the original spherical waves, diffraction takes place in the hologram in such a way that the original plane waves are reconstructed. In this situation, the HOE performs like a collimating lens. Similarly, when the HOE is illuminated by the conjugate plane waves, i.e. traveling opposite to their original direction, then the conjugate spherical waves, i.e. converging as opposed to originally diverging, are reconstructed. For this case, the HOE performs as an optical-transforming lens. As is typical of holography, certain factors are required during HOE formation, whereby

(reconstructed wave intensity) $\propto$ (interference fringe contrast) $\propto$ (HOE diffraction efficiency)

is maximized. Both spherical and plane waves must (1) propagate in phase with the same wavelength, (2) have constant flux, and (3) have linear polarization vectors, (E), which are always parallel to the plane of the hologram. In addition, the hologram medium must render a linear recording of the interference amplitudes.

Inline and off-axis hologram configurations represent two possible HOE models. The inline model in figure 4 denotes U, V as the plane of interference. The plane wavefronts propagating from the point (0, 0, $-\infty$) constitute planar surfaces of constant phase as defined by the complex amplitude R:

$$R = R(x,y,z,) = R_o \exp [i (\vec{k}_1 \cdot \vec{r}_1)]$$

where $\vec{k}_1 \cdot \vec{r}_1 = k z$.

$$\left|\vec{r}_1\right| = z$$

The diverging spherical wavefronts originating from the point (0, 0, 0) constitute spherical surfaces of constant phase as defined by the complex amplitude S:

$$S = S(x,y,z) = \frac{S_o \exp [i (\vec{k}_2 \cdot \vec{r}_2)]}{\left|\vec{r}_2\right|}$$

where $\vec{k}_2 \cdot \vec{r}_2 = k r$

$$\left|\vec{r}_2\right| = r$$

The pattern of concentric circles in the U, V plane (figure 4) represents maximum interference resulting from the linear superposition of R and S. The resultant intensity

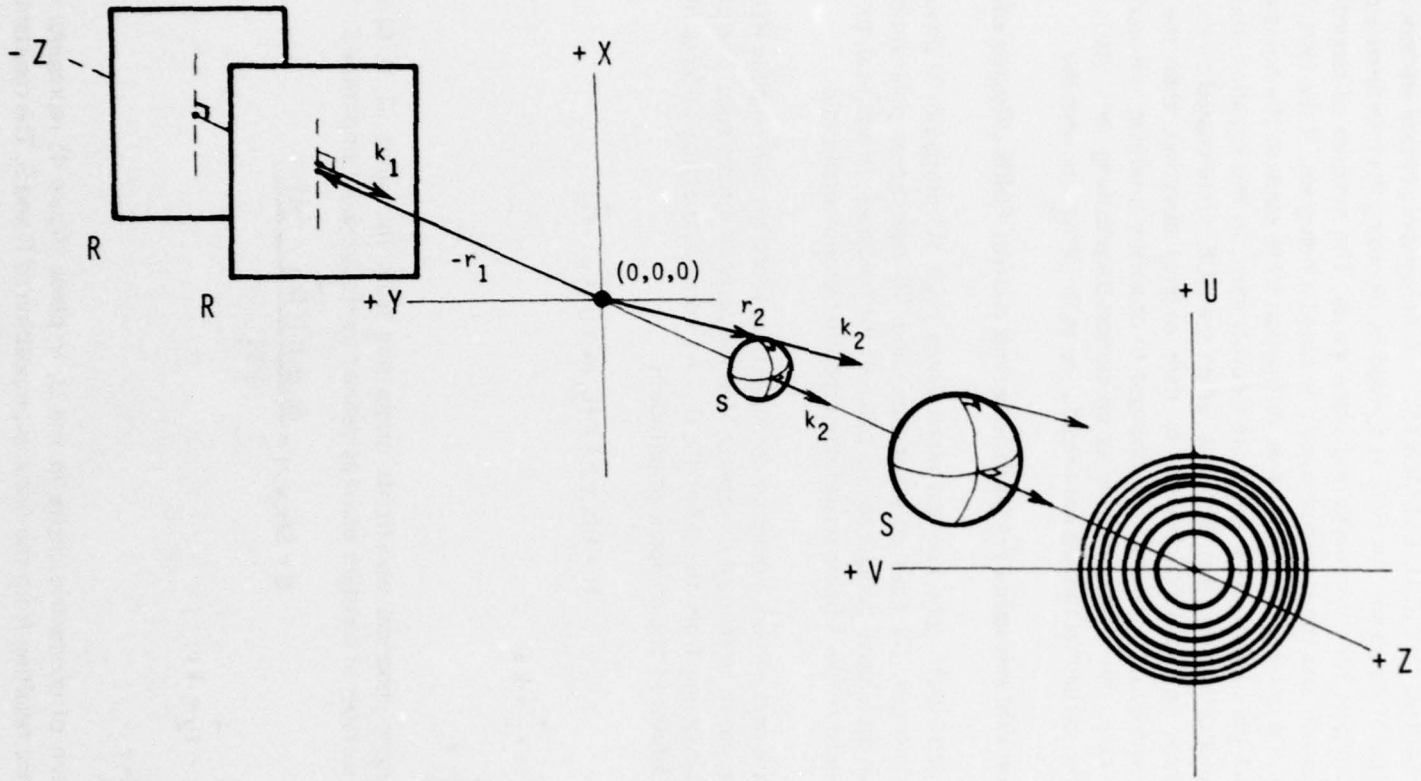

Figure 4. Inline Hologram Configuration

variation I,

$$I(u,v) = (R + S)(R^* + S^*)$$

$$= R_o^2 + \left(\frac{S_o}{r}\right)^2 + \left(\frac{2R_o S_o}{r}\right)\cos[kr - kz]$$

$$I(\rho) = R_o^2 + \left(\frac{S_o^2}{\rho^2+f^2}\right) + \left(\frac{2R_o S_o}{\sqrt{\rho^2+f^2}}\right) G(\rho)$$

where $G(\rho) = \cos[k(\sqrt{\rho^2 + f^2} - f)]$

$$r^2 = \rho^2 + f^2$$

$$\rho^2 = u^2 + v^2$$

$$f^2 = z^2 = \text{constant} = \textbf{focal length}$$

yields three terms; the first being constant, the second essentially constant for $f^2 >> \rho^2$, and the third radially cosinusoidal. Figure 5 illustrates the cosinusoidal variation of the third term as $0 \leq \rho \leq 4.0$ millimeters for particular values of f, λ, R_o and S_o. Obviously, this differs from the radial square-wave intensity variation found in a FZP that would otherwise be formed by Fresnel zone construction owing to S alone.

Similarities between the FZP and the inline HOE construction may be examined for the simple case in which $f = \lambda$. Figure 6 places the U, V plane at (u,v,f) and uses a series of parallel planes at $Z = \lambda, 2\lambda, 3\lambda, \ldots 7\lambda$ to more easily illustrate the microscopic wave interference effects. Fresnel zone construction for P (0,0,0) and P' (0,0,∞) requires that all the dots denote maximum intensity at the intersection of spherical waves (S) and the U, V and for the corresponding parallel planes for all incremental $\lambda/2$ distances from P (0,0,0) within the volume U-V-Z where $\lambda \leq z \leq 7\lambda$. In the case of HOE construction, however, an intensity pattern is formed owing to the interference between R at (0,0, - ∞) and S at (0,0,0). Thus, only the circled dots will denote maximum intensity for the eight parallel planes within U-V-Z. (Recall that the circled dots in one plane relate to points on the maximum circular lines in the U, V plane previously shown in figure 4.) If this approach is continued, an infinite number of planes are considered parallel to the U, V plane in space and within U-V-Z (figure 7). The resulting maximum points lie along lines that represent a series of parabolic functions having the same focus, (0,0,0). Note that this concept could easily be extended to examine the more practical case in which $z \sim (10^5 \lambda) \sim 200$ millimeters.

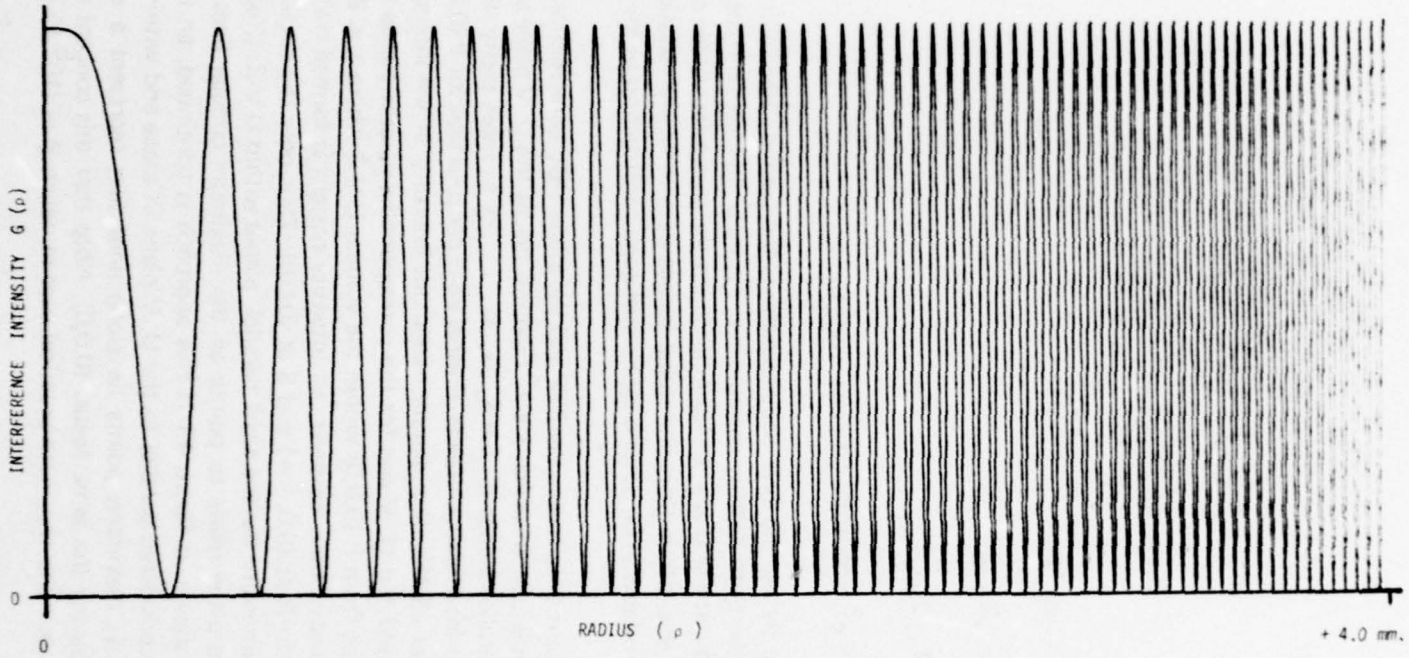

Figure 5. Interference Intensity Along a Radial Axis.

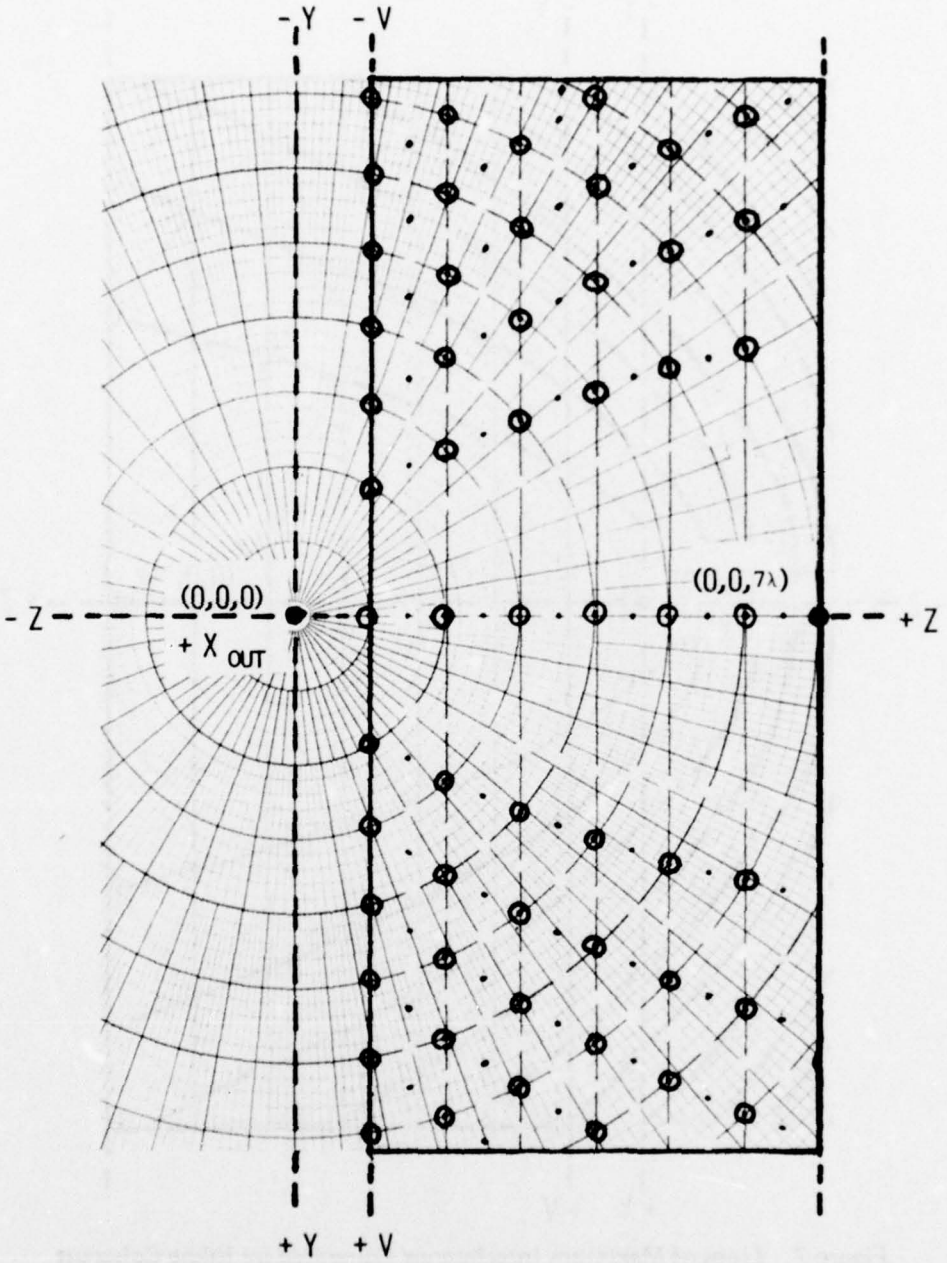

Figure 6. Points of Maximum Interference Between Inline Coherent Spherical and Plane Waves Within Volume of Thickness T.

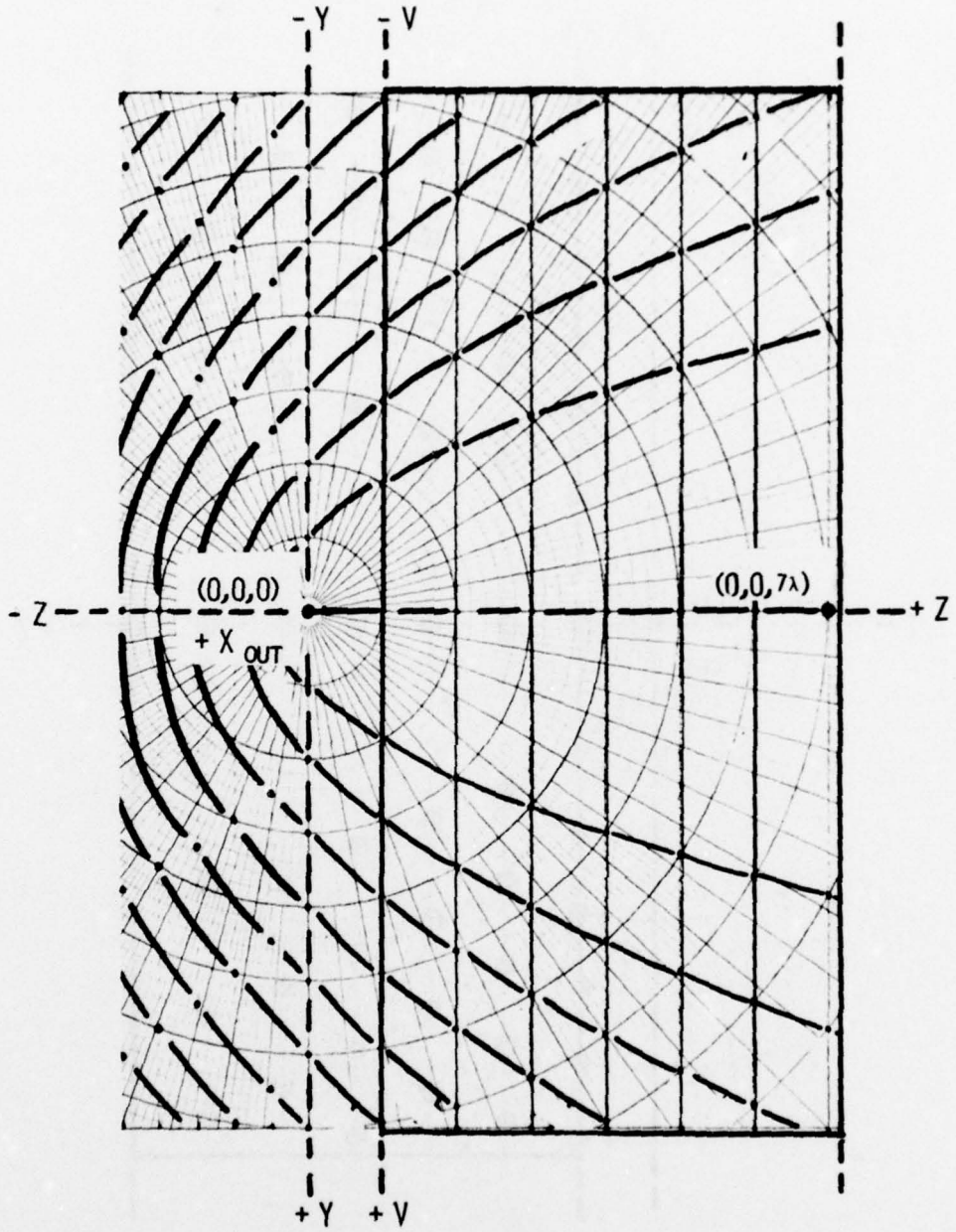

Figure 7. Lines of Maximum Interference Generated by Inline Coherent Spherical and Plane Waves Within All Space.

In practice, an off-axis HOE is more viable than an inline HOE. Conceptually, there is very little difference between both approaches. The off-axis model, figure 8, shows R intersecting the U, V plane at an angle ψ. The plane wavefronts propagating from the point (0, - y, - ∞) constitute planar surfaces of constant phase as defined by the complex amplitude R':

$$R' = R'(x,y,z) = R_o \exp [i (\vec{k}_1 \cdot \vec{r}_1)]$$

where $(\vec{k}_1 \cdot \vec{r}_1) = k[y \sin \psi + z \cos \psi]$
with the interbeam angle $\psi = \tan^{-1} (k_y/k_z)$ (1)

Again, the diverging spherical wavefronts originating from the point (0,0,0) constitute surfaces of constant phase as defined by the complex amplitude S':

$$S' = S'(x,y,z) = \frac{S_o \exp [i \vec{k}_2 \cdot \vec{r}_2)]}{|\vec{r}_2|}$$

where $\vec{k}_2 \cdot \vec{r}_2 = k \quad r$
$|\vec{r}_2| = r$

The pattern of asymmetric circles in the U, V plane, figure 8, represent maximum interference resulting from the linear superposition of R and S. The resultant intensity variation I',

$$I' = I'(u,v) = (R + S)\ (R^* + S^*)$$

$$I'(x,y) = R_o^2 + \left(\frac{S_o}{r}\right)^2 + \left(\frac{2 R_o S_o}{r}\right) \cos [kr - k(y \sin \psi + z \cos \psi)]$$

$$I'(\rho) = R_o^2 + \left(\frac{S_o^2}{\rho^2 + f^2}\right) + \left(\frac{2 R_o S_o}{\sqrt{\rho^2 + f^2}}\right) G'(\rho) \qquad (2)$$

where $G'(\rho) = \cos [k(\sqrt{\rho^2 + f^2} - y \sin \psi - f \cos \psi)]$
$r^2 = \rho^2 + f^2$
$\rho^2 = u^2 + v^2$
$f^2 = z^2 =$ focal length

yields three terms; the first being constant, the second essentially constant for $f^2 >> \rho^2$ and the third (asymmetrically) radially cosinusoidal. Figures 9 and 10 illustrate the

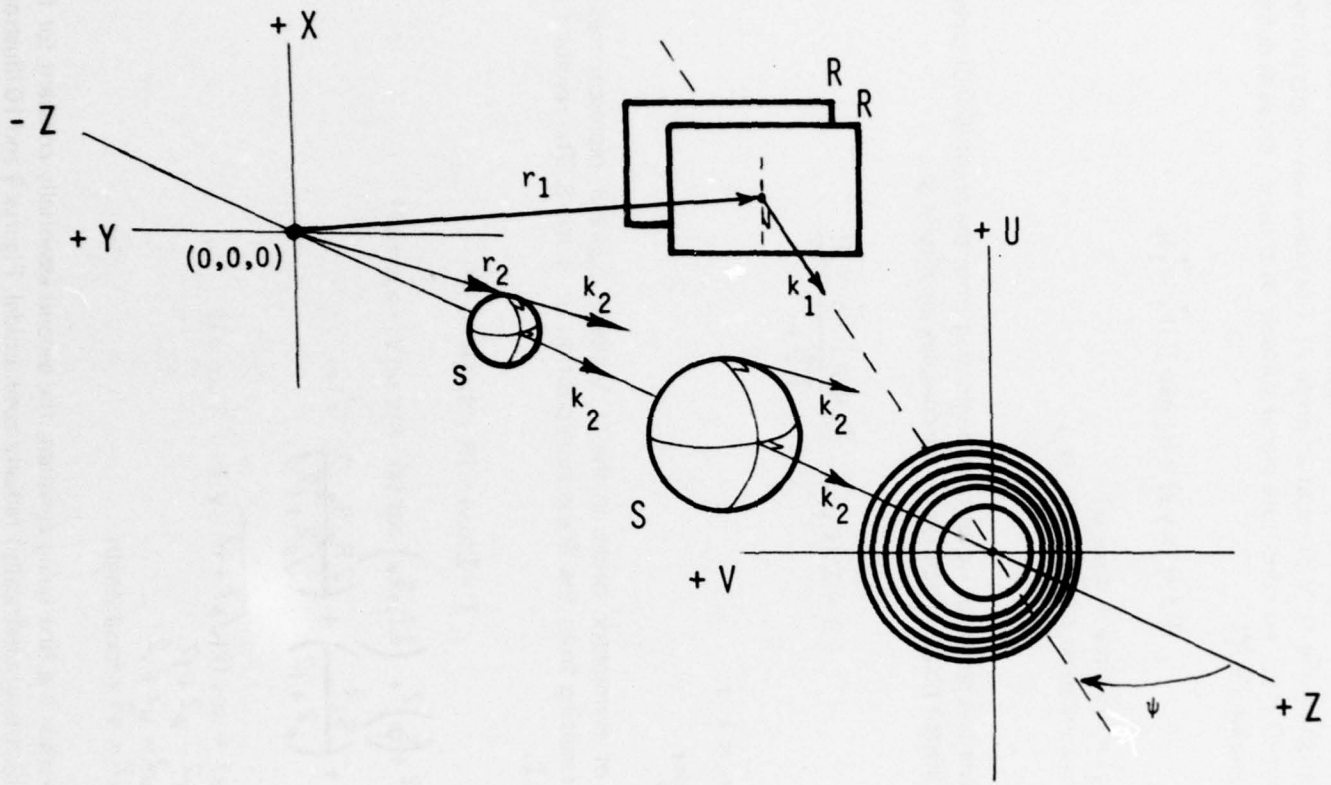

Figure 8. Off-Axis Hologram Configuration.

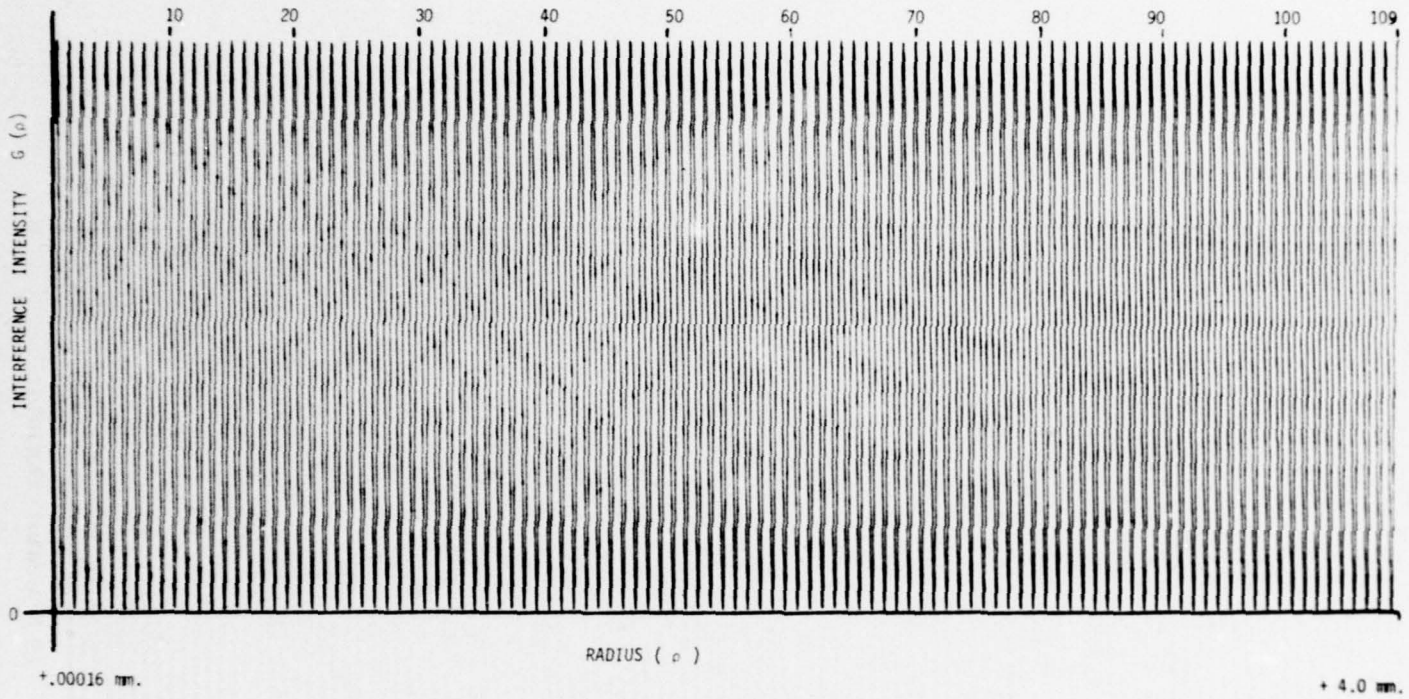

Figure 9. Interference Intensity Along the +V Axis.

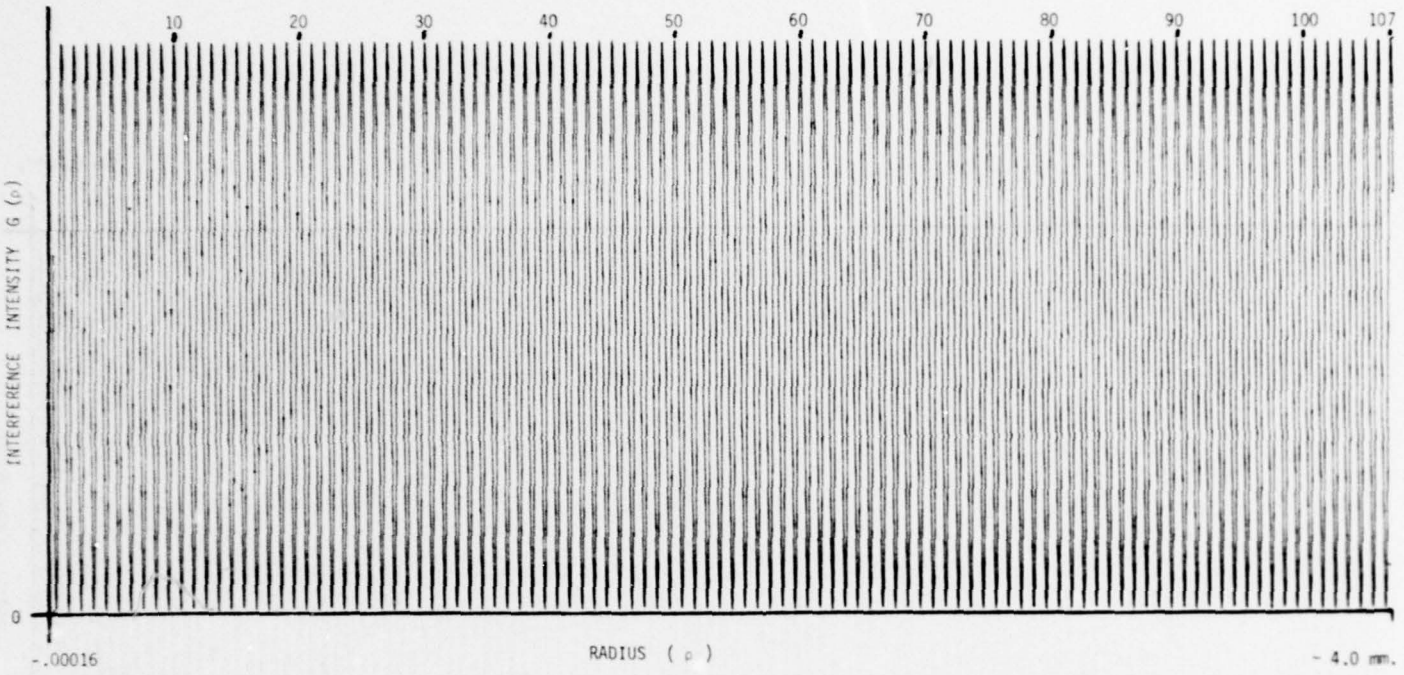

Figure 10. Interference Intensity Along the -V Axis.

asymmetrical cosinusoidal variation of the third terms as $0 \leq \rho \leq 4.0$ millimeters for particular values of f, λ, R_o, S_o, and ψ. Note that figure 9 illustrates ~ 109 cycles in the +V direction for $\rho = +v = 4.0$ millimeters as opposed to ~ 107 cycles in the -V direction for $\rho = -v = -4.0$ millimeters for figure 10. The asymmetry is directly related to the value of ψ.

Similarities between an FZP and an off-axis HOE construction are examined for the case in which $f = \lambda$. Figures 11 and 12 are analagous to figures 6 and 7 in the previous comparison between an FZP and an inline HOE. Again, this case can be easily extended to examine a more practical case in which $Z \sim 10^5 \lambda \sim 200$ millmeters.

LOW Q-FACTOR HOLOGRAPHIC OPTICAL ELEMENTS. The low Q-factor holographic optical element is a special type of off-axis HOE. Its diffraction properties exhibit minimal angular sensitivity and near-maximum diffracted first-order intensity. In effect, the low Q-factor HOE is a combination of a thin and thick hologram with the preferred diffraction properties of both.

Recall that a hologram initially formed by the interference of two plane waves has discrete diffraction properties that are a function of the factor Q:

$$Q = 2 \pi \lambda T / nd^2 \qquad (3)$$

where λ = wavelength of light source
T = recording medium thickness
n = medium index of refraction
d = spacing between amplitude maxima

In this general case, a sinusoidal amplitude/phase variation is recorded in the plane of interference along one direction. Upon reconstruction, the light is diffracted into only the 0 and the ± 1 orders. In practice, however, there are nonlinearities in the recording media that introduce components of a Fourier series of the fundamental sinusoid. The presence of these components gives rise to additional diffraction orders upon reconstruction.

When $Q \geq 10$, the medium is considered thick (i.e. three-dimensional) and thus exhibits diffraction characteristics of a volume grating as described by the Bragg equation:

$$m\lambda = 2 d (\sin \beta)$$

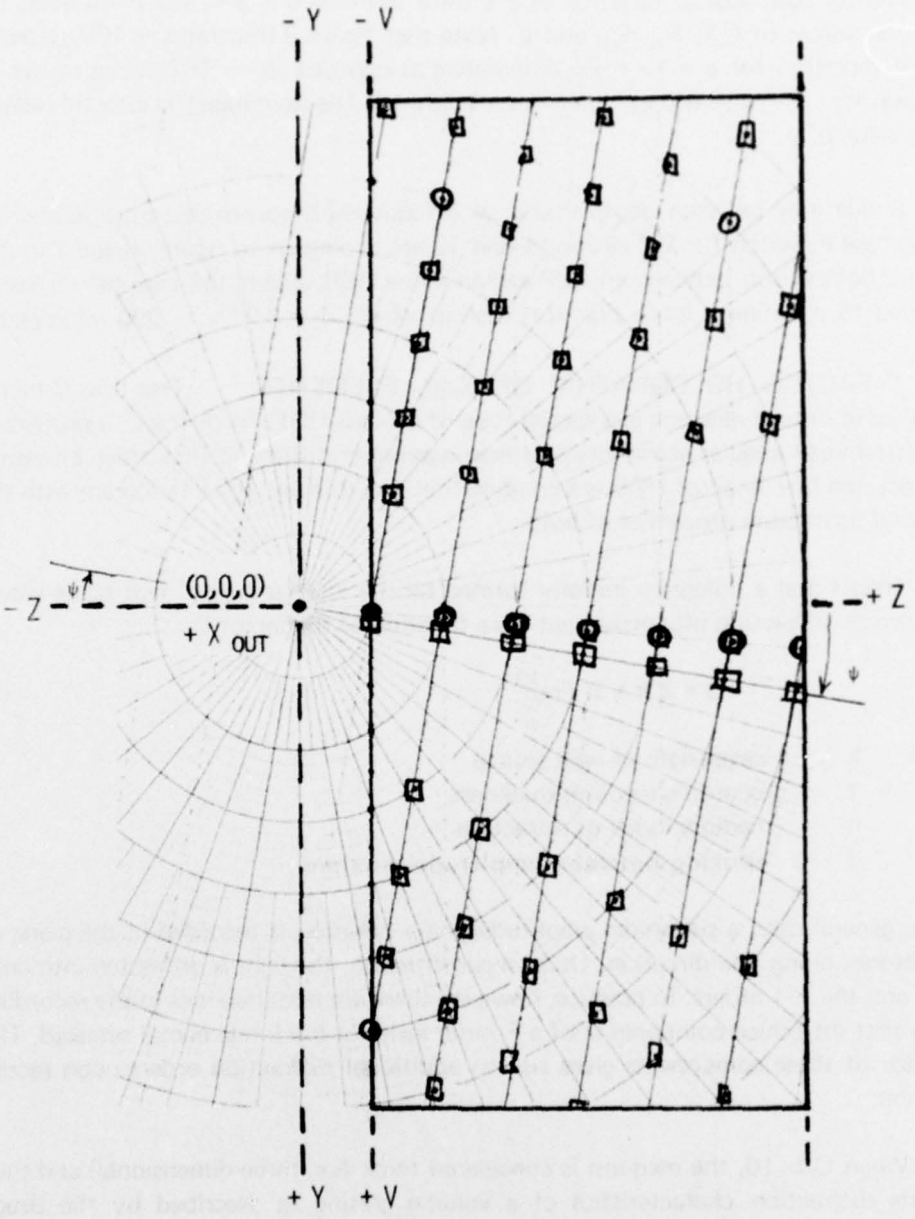

Figure 11. Points of Maximum Interference Between Coherent Spherical and Plane Waves (Separated by ψ) With a Volume of Thickness T.

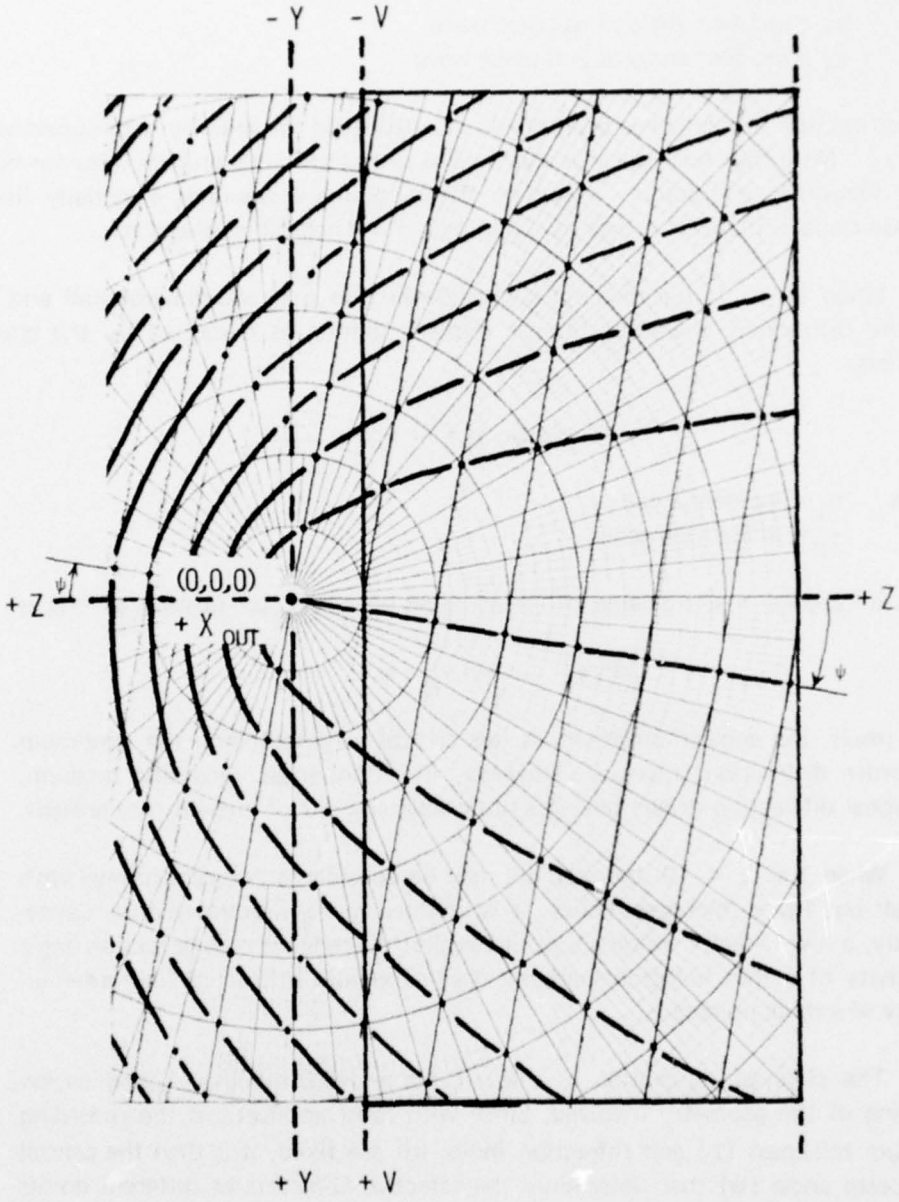

Figure 12. Lines of Maximum Interference Generated by Coherent Spherical and Plane Waves (Separated by ψ) Within All Space.

where $\beta = (\alpha_1 + \alpha_2)/2$ = incident and diffraction angle
α_1 = incident angle of lst plane wave
α_2 = incident angle of 2nd plane wave

This diffraction property has been previously described in detail by the coupled wave theory.[11] Note that for a given λ and d value, β has only one angular value for maximum first-order diffraction. Assuming the recording material is essentially linear, any additional diffraction orders have minimal, if not negligible, intensity.

When $Q < 1$, the medium is considered thin (i.e. two-dimensional) and thus has the diffraction characteristics of a plane grating as described by the grating equation:

$$m\lambda = d(\sin \gamma_i + \sin \gamma_d)$$

where γ_i = incident angle
γ_d = diffraction angle

Thus, for a given λ and d value, different values of γ_i or γ_d are possible as long as

$$\left|\sin \gamma_i\right| \ , \ \left|\sin \gamma_d\right| \leq 1.$$

As a result, the angular sensitivity is less critical in determining the maximum first-order diffraction intensity. However, in a nonlinear recording medium, additional diffraction orders having a noticeable amount of intensity are present.

When $1 \leq Q < 10$, the medium may be considered two-dimensional with a small but finite thickness; hence, it is denoted quasi-two-dimensional. Consequently, a low Q-factor hologram would exhibit the reduced reconstruction angle sensitivity of a thin hologram and the near maximum diffracted first-order intensity of a thick hologram.

The physical conception of a low Q-factor HOE requires a good understanding of the geometry involved. Since with most applications the recording medium thickness (T) and refraction index (n) are fixed, it is then the central interbeam angle (ψ) that determines the effective Q-factors at different points in the hologram plane. The limiting angles

[11] H. Kogelnik, "Coupled Wave Theory for Thick Hologram Gratings," *Bell System Tech. J.*, Vol. 48, 1969, p. 2909.

$$\tau = \psi - \phi \tag{4}$$

$$\kappa = \psi + \phi \tag{5}$$

$$\xi = \cos^{-1}\left[\frac{\cos^2\psi + \cos^2\phi - 1}{\cos\psi\ \cos\phi}\right] \tag{6}$$

where $= \tan^{-1}\left[\frac{r_o}{f\cos\psi}\right]$ (7)

are obtained from the geometry of the HOE diagrams in figures 13 and 14. By assuming any small area of the $\vec{S}$ wavefront to be essentially planar, the interference between $\vec{R}$ and $\vec{S}$ can be viewed at any single point in the U, V plane as plane wave interference. Thus, if $(0, v_\tau, f)$, (0,0,f), $(0, -v_\kappa, f)$ and $(u_\xi, 0, f)$ denote the vertices of τ, ψ, κ, and ξ, respectively, then the interfringe spacing at each point is

$$d_\tau = \lambda \ / \ 2\sin(\tau/2) \tag{8}$$

$$d_\psi = \lambda \ / \ 2\sin(\psi/2) \tag{9}$$

$$d_\kappa = \lambda \ / \ 2\sin(\kappa/2) \tag{10}$$

$$d_\xi = \lambda \ / \ 2\sin(\xi/2) \tag{11}$$

From this, the effective Q-factors and spatial frequency (i.e. 1/d) at each point in the U, V plane would be calculable.

EXPERIMENTAL TECHNIQUES

The design modeling and physical construction of low Q-factor holographic optic elements (HOE) was done in iterative steps. The purpose of this procedure was to optimize the total optical performance of the HOE.

HOLOGRAM CONSTRUCTION. A series of low Q-factor holographic optical elements (HOE) having a 50-millimeter clear aperature of f/4.3 were constructed with .6328-micrometer laser light. Although smaller f-numbers were desirable, a minimum focal length of 215 millimeters was necessary to accommodate the small interbeam angle (ψ) of 9.8 degrees (see figure 13). By using equations 1 and 3 through 11, the spatial frequency requirements and respective Q-factors at the vertices (see figure 13 and 14), τ, ψ, κ, and ξ are

$$d_\tau = 85\ 1/\text{mm} \quad ' \qquad Q_\tau = 0.285$$

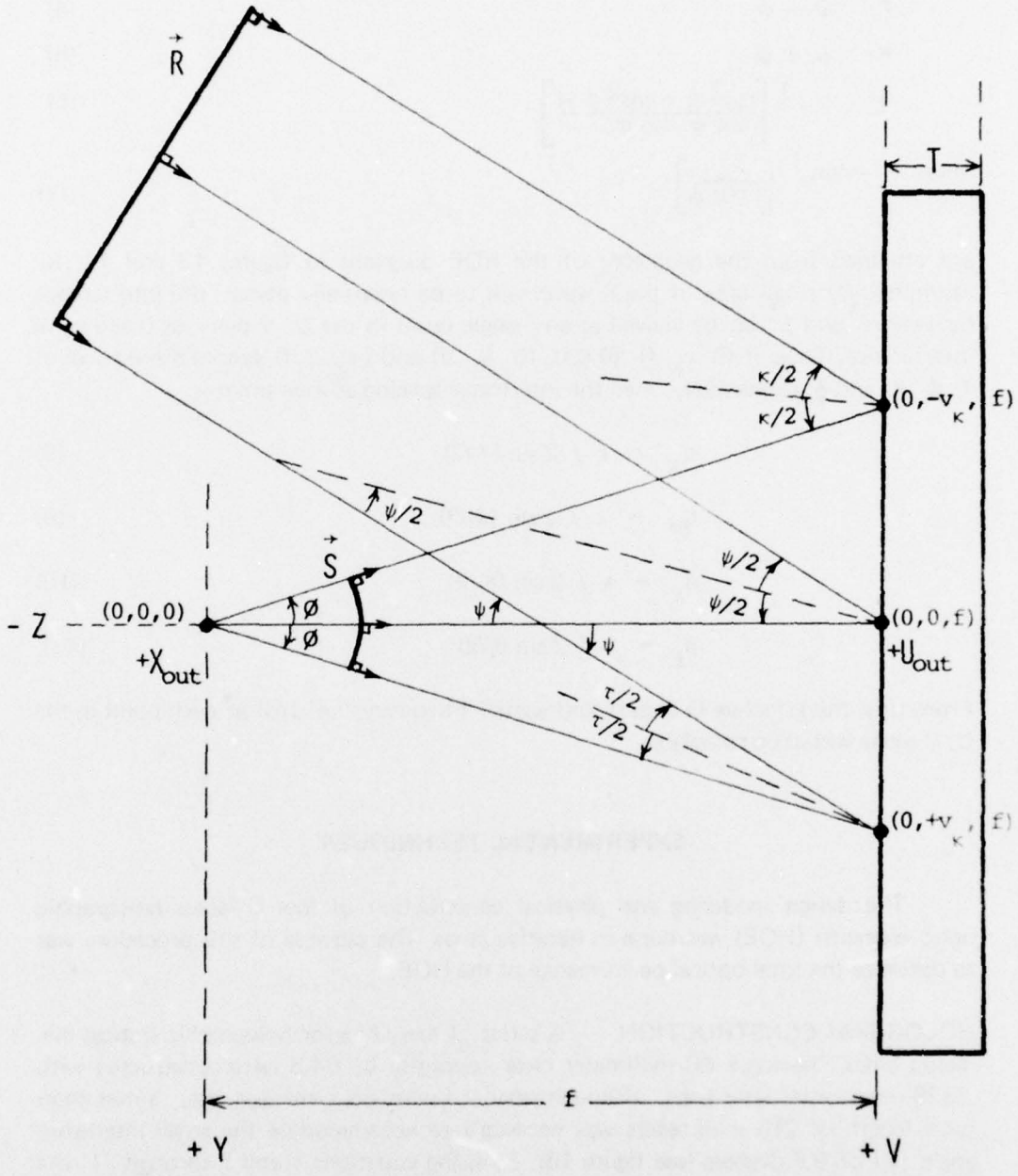

Figure 13. Geometry of Holographic Optical Element Construction (Y – Z View).

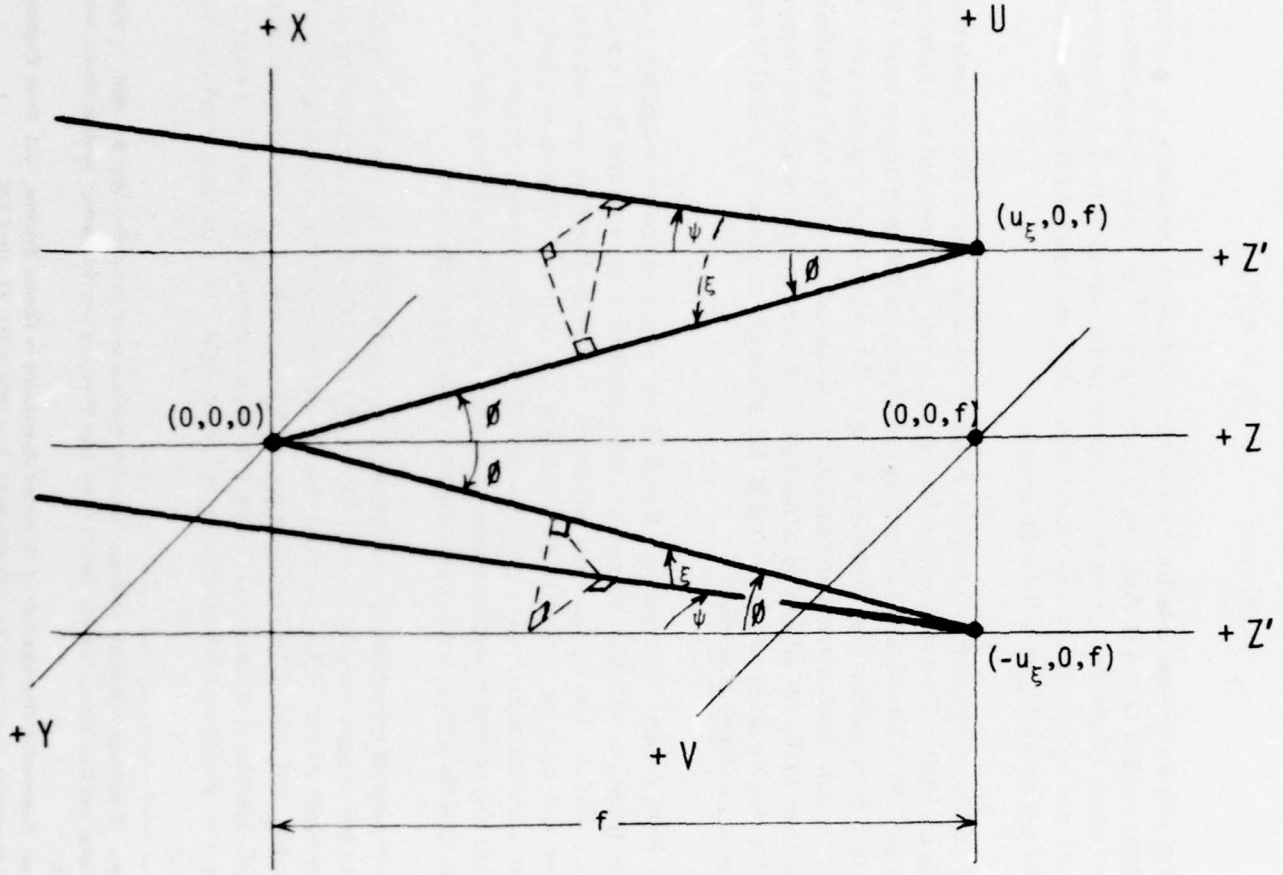

Figure 14. Geometry of Holographic Optical Element Construction (X-Y-Z View).

$$d_{\psi} = 270\ 1/mm \quad ' \qquad Q_{\psi} = 2.90$$

$$d_{\kappa} = 454\ 1/mm \quad ' \qquad Q_{\kappa} = 8.20$$

$$d_{\xi} = 330\ 1/mm \quad ' \qquad Q_{\xi} = 4.33$$

Computing an average Q-factor for the five points at the vertices τ, κ, ψ, ξ-top, and ξ-bottom yielded $\bar{Q} = 4.0$. Applying $\bar{Q}$ to the graph[12] in figure 15 established a theoretical limit of 60 percent for the first-order of diffracted intensity (I_1). Since only 9 percent of the light intensity was undiffracted (I_o), the balance (31 percent) was then distributed among higher diffraction orders.

The optical components illustrated in figure 16 were used in the construction of low Q-factor HOE's. The plane wave reference beam (R) was generated by a Spectra-Physics model 336, 50-millimeter collimating lens. The spherical wave subject beam (S) was generated by a spatial filter assembly using a 40X microscope objective and a 4-micrometer pinhole. Each mirror and beam splitter surfaces had optical path deviations (OPD) less than $\lambda/20$. An air-vented, stray-light trap surrounded the Spectra-Physics model 124A He–Ne laser, which produced 15 milliwatts of vertically (1,000:1) polarized light at $\lambda = .6328$ micrometer.

The HOE's were recorded on Kodak 649F emulsion-coated microflat glass plates. The backside (air-glass boundary) was coated with an antireflection coating provided by Kodak. The plates were processed in SD-48 developer and reversally bleached in R-9 bath as indicated by Lamberts and Kurtz.[13] Maximum values of 50 percent were measured for the first-order diffraction efficiency. Previous HCP work[14] with this reverse bleaching process had also yielded reasonably high diffraction efficiencies, low flare light, and a great resistance to print-out darkening.

The measured intensities of the reference (I_r) and subject (I_s) beams were used to compute the radially varying K-ratios ($K = I_r/I_s$) of 1.50 and 1.00 at the center and edge respectively of the HOE aperature. Maximum exposure was computed at $t = 2$ seconds and $I_E = 0.405, 0.18$ (milliwatt per square centimeter) at the center and edge of the HOE aperature, respectively. Since the linear superposition principle must be applied to the amplitudes of interfering coherent light, the exposure intensity was calculated as

---

[12] W.R. Klein, "Theoretical Efficiency of Bragg Devices," *Proceedings of the IEEE*, Vol. 54, 1966, P. 803.

[13] R.L. Lamberts and C.N. Kurtz, "Reversal Bleaching for Low Flare Light in Holograms," *Applied Optics*, Vol. 10 1971, P. 1342.

[14] W.R. Graver, *Holographic Compensation of Wavefront Aberrations in Optical Systems*, U.S. Army Engineer Topographic Laboratories, Fort Belvoir, Va., ETL-RN-74-11, June 1975, NTIS: AD-A013 978.

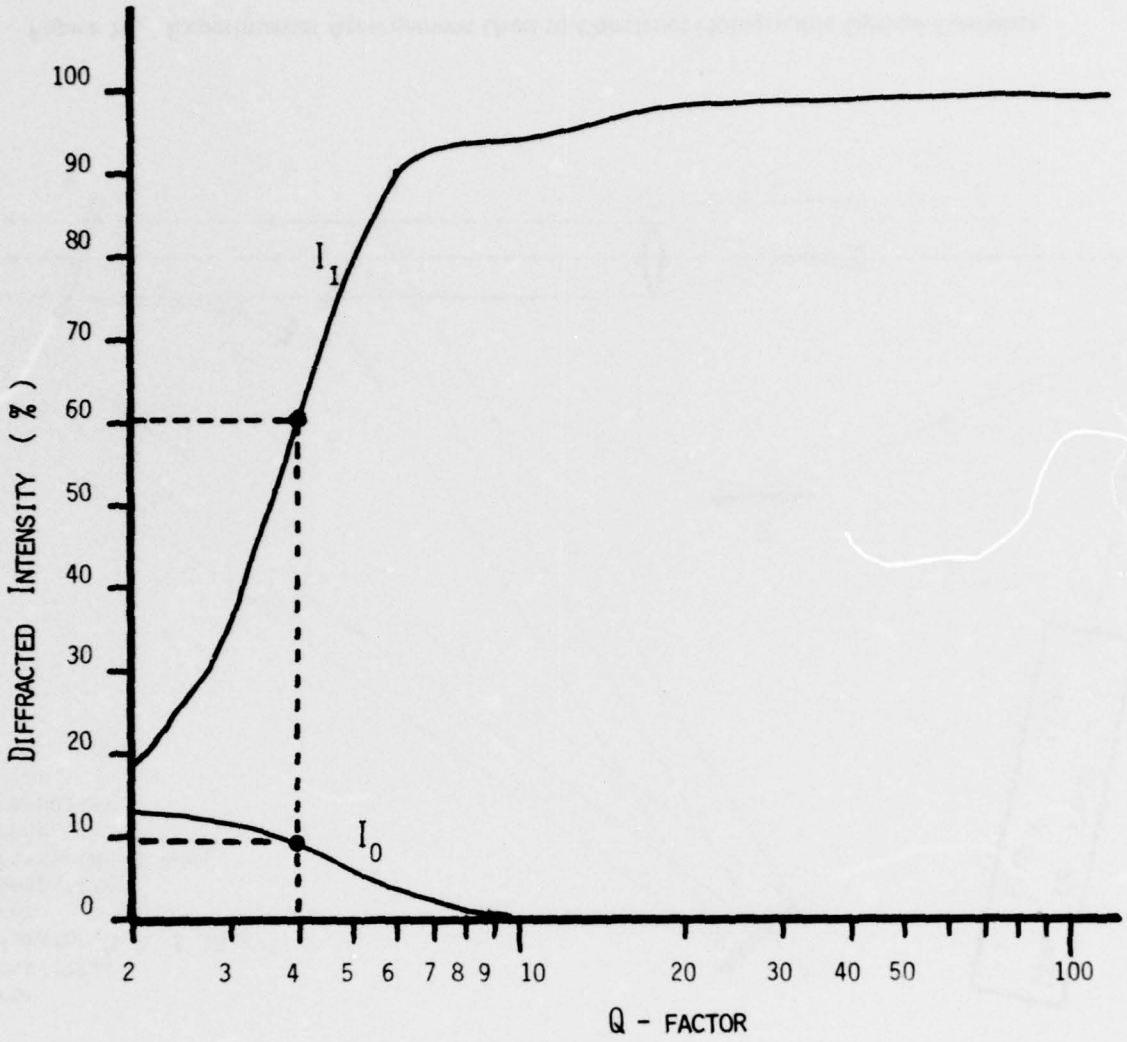

Figure 15. First-Order Diffracted Intensity Vs. Q-Factor.

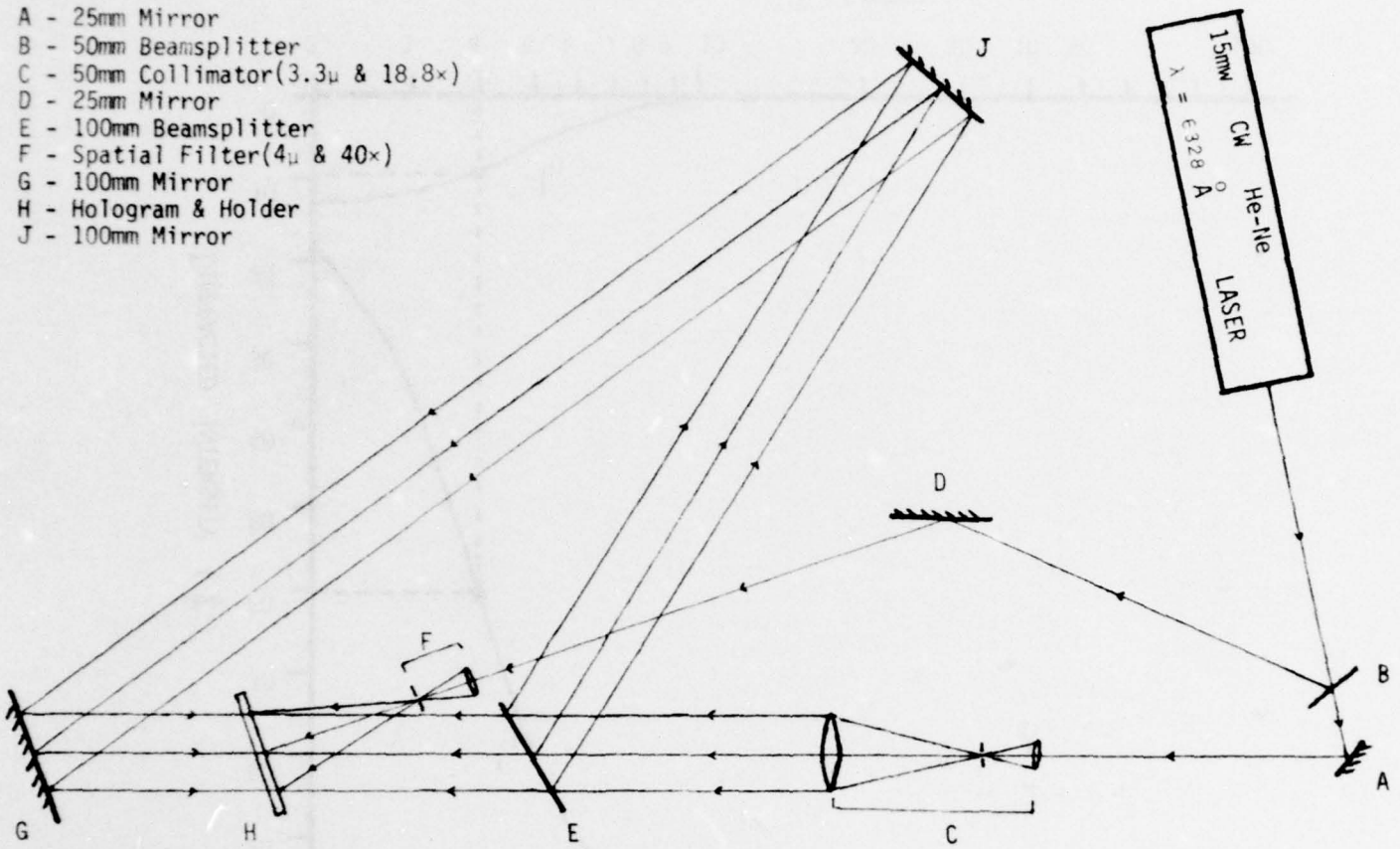

Figure 16. Experimental Arrangement Used to Construct Holographic Optical Elements.

$$I_{E\,max} = I_r + I_s + 2\,(I_r I_s)^{1/2}$$

$$I_{E\,min} = I_r + I_s - 2\,(I_r I_s)^{1/2}$$

where $\Delta I_E = I_{E\,max} - I_{E\,min}$

$= 4\,(I_r I_s)^{1/2}$ for interference fringe contrast

A computer plotter was used to develop (figure 17) the radially decreasing K-ratio (K_β) present in the experiment. (The curve K_a is a theoretical construct that is possible only when both plane and spherical wavefronts have a uniform intensity distribution.) Although differences between the nearly constant K_a and the gaussian-shaped K_β at ρ = 25 millimeters was greater than desired, it was unavoidable in practice.

During hologram construction, an optical stop was placed between G and J (figure 16). This enabled only the plane waves (R) propagating from E to H to interfer with the spherical waves generated at F. Exposing the 649F emulsion for time (t) with various intensity values ($I_{E\,max}$) produced a series of six holographic optical elements.

WAVEFRONT RECONSTRUCTION. After exposure and subsequent photo-reversal processing, the HOE was repositioned in its holder. Under the constant illumination from both spherical and wavefronts, fine orientation adjustments were made to the holder to minimize any Moire' fringes observed on the HOE owing to emulsion distortions or shrinkage. The success of this Moire' repositioning procedure was discussed in previous work.[15]

Reconstruction of the pinhole source (S) was accomplished by placing optical stops between $\overline{H\ E}$ and $\overline{D\ B}$. By this process, the original intensity pattern of the HOE (equation 2) would be modulated by R^* such that

$$(R^*)\,I' = R^*\,(I_r + I_s) + I_r S^* + (R^*)^2 S$$

where $I_r S^*$ is a converging spherical wavefront with I_r intensity. The airy-disk diffraction pattern in figure 18 was recorded on Kodak Panatomic-X film in the plane of the pinhole. However, the dynamic recording range required by the associated intensity

---

[15] W.R. Graver, *Holographic Compensation of Wavefront Aberrations in Optical Systems*, U.S. Army Engineer Topographic Laboratories, Fort Belvoir, Va., ETL-RN-74-11, June 1975, NTIS: AD-A013 978.

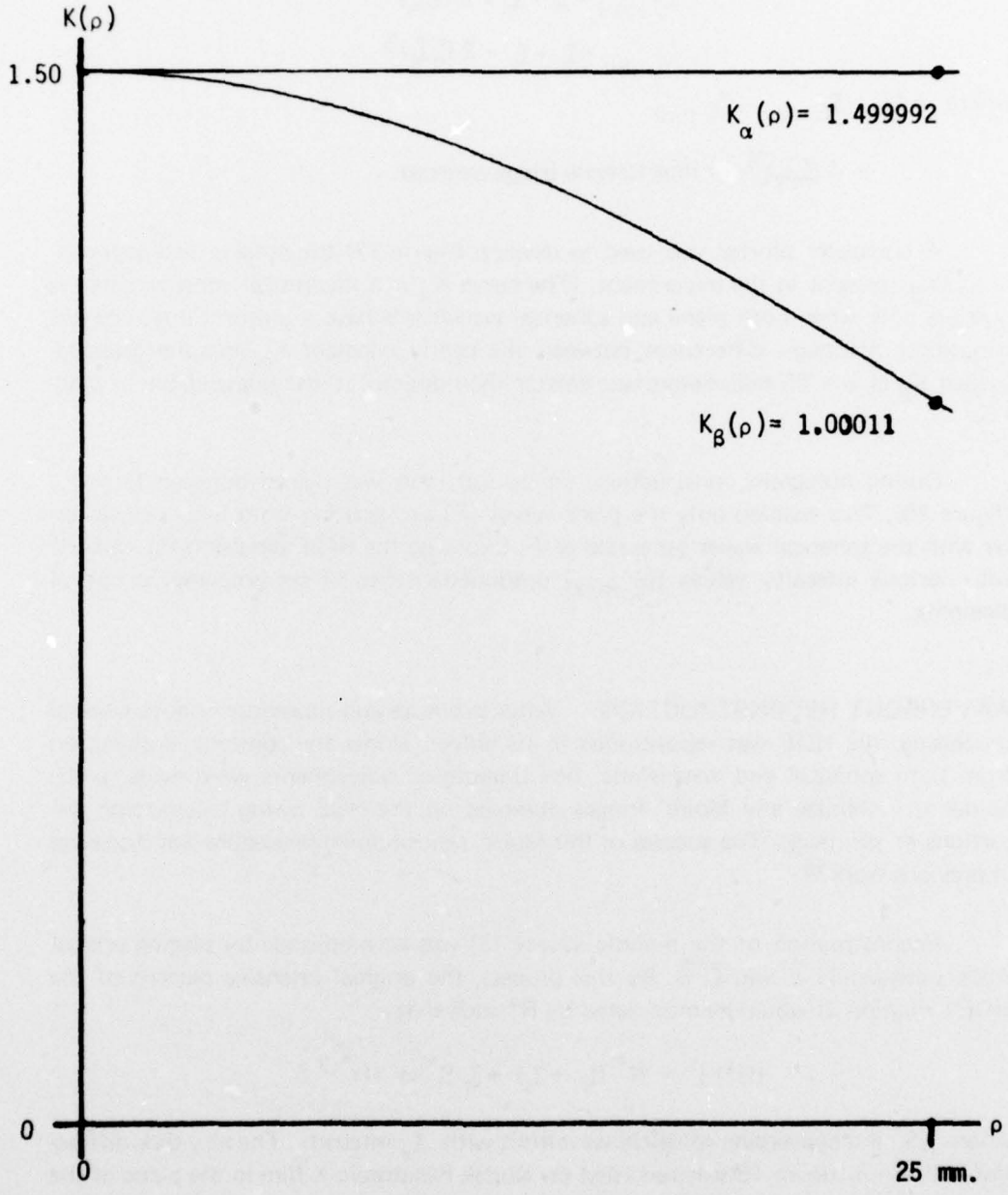

Figure 17. Comparison of Gaussian and Uniformly Distributed K-Ratios.

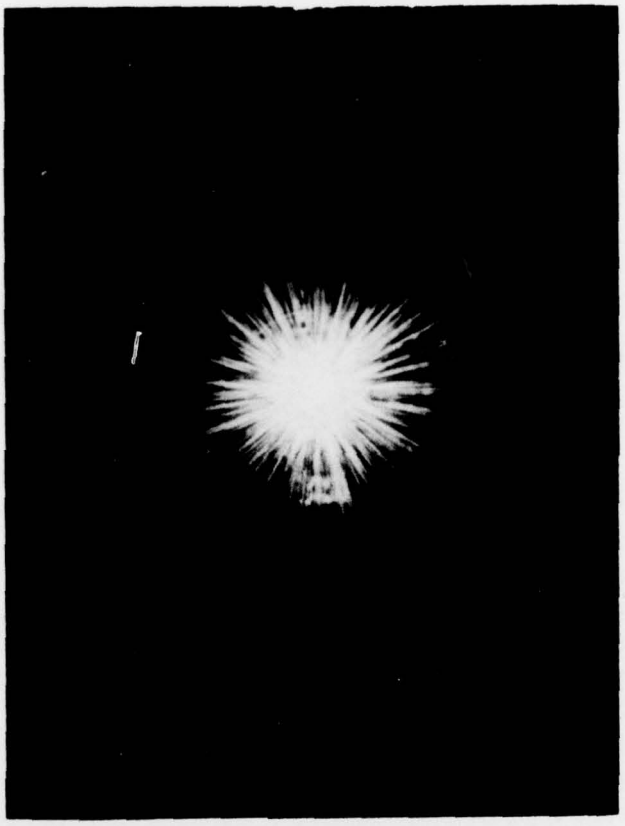

Figure 18. Diffraction Pattern Generated by a Holographic Element.

distribution $2[J_1(\rho) / \rho]^2$ was beyond the range of the recording film. Since dynamic range limitations presently exist with all silver-gram emulsions, this approach could not be used as an accurate quantitative measurement of wavefront reconstruction.

Reconstruction of the reference wavefront (R) was accomplished by placing an optical stop between $\overline{B\ A}$. By this process, the original intensity pattern of the HOE would be modulated by S such that

$$(S)\, I' \approx S\,(I_r + I_s) + I_s R \approx (S)^2\, R^*$$

where $I_s R$ is a plane wavefront with I_s intensity.
Unfortunately, the optical layout (figure 16) provided no method for measuring the OPD of the reconstructed wavefronts. Since the Sagnac[16] (cyclic) interferometer between components E, G, and J determined only the tilt alignment between R^* (traveling along E-J-G-H) with R (traveling along E-H), a different type of interferometer was needed.

OPTICAL PERFORMANCE EVALUATION

A novel laser alignment procedure was developed and used to generate interferograms of holographic optical elements.[17] The interferograms were obtained with a Zygo interferometer, (model GH, Zygo Corp) which is specified to have a $\lambda/20$ optical path deviation in double-pass accuracy using an internal He–Ne laser. Since the interferometer was used in a double-pass configuration, the measured path deviation is one-half of the observed fringe variation in the interferograms illustrated here. Although easy to use when testing conventional lenses, the asymmetry present in the holographic elements complicated the basic alignment procedure of the interferometer, thus requiring many alignment iterations.

Initially, it was necessary to test the interferometric quality of the glass microflats since the quality varies.[18] A series of sample microflats were obtained by removing the emulsion in a sulfuric acid bath. Placing a sample microflat normal to the optical axis of the interferometer (figure 19) produced an interferogram (figure 20) showing the effective wedge angle and the phase contributions present. Measuring the other samples in a series yielded similar results.

---

[16] W.H. Steel, *Interferometry*, Cambridge University Press, London, 1967, P. 94.

[17] W.R. Graver, "Interferograms of Holographic Optical Elements," *J. Applied Optics*, Vol. 16, 1977, P. 1809.

[18] Eastman Kodak Co., *Physical Characteristics of Glass for Kodak Photographic Plates*, Publication No. Q-35, Rochester, N.Y., 1973.

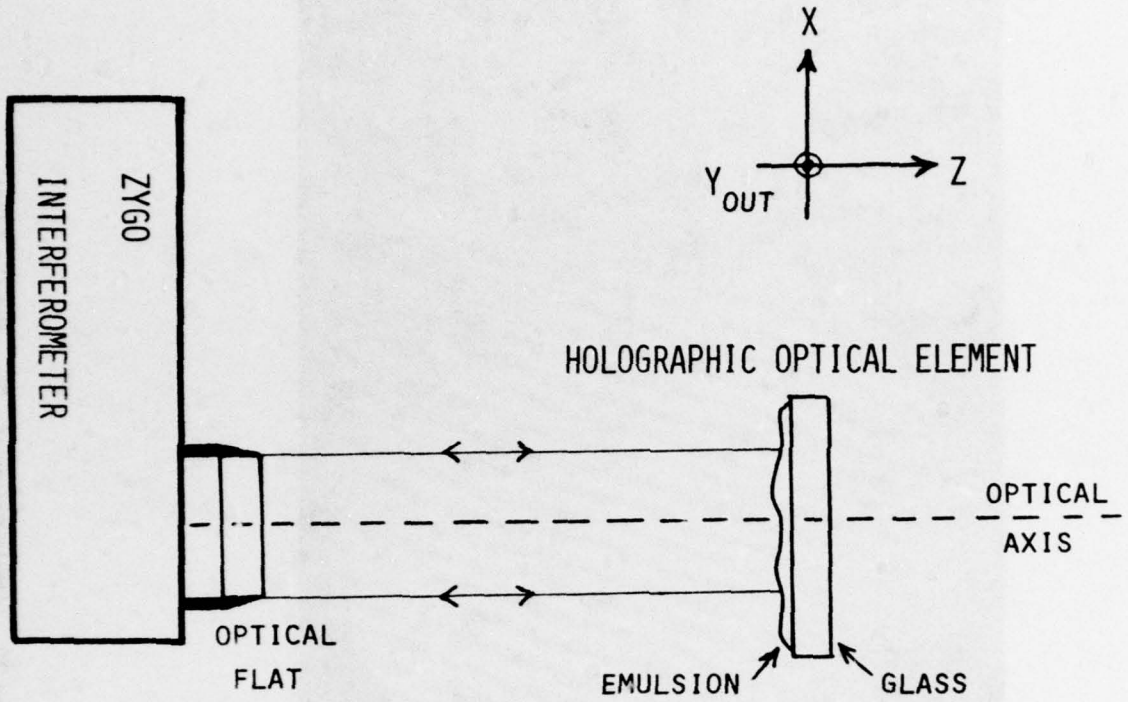

Figure 19. Experimental Arrangement Used to Produce Figures 20, 21, 22, and 23.

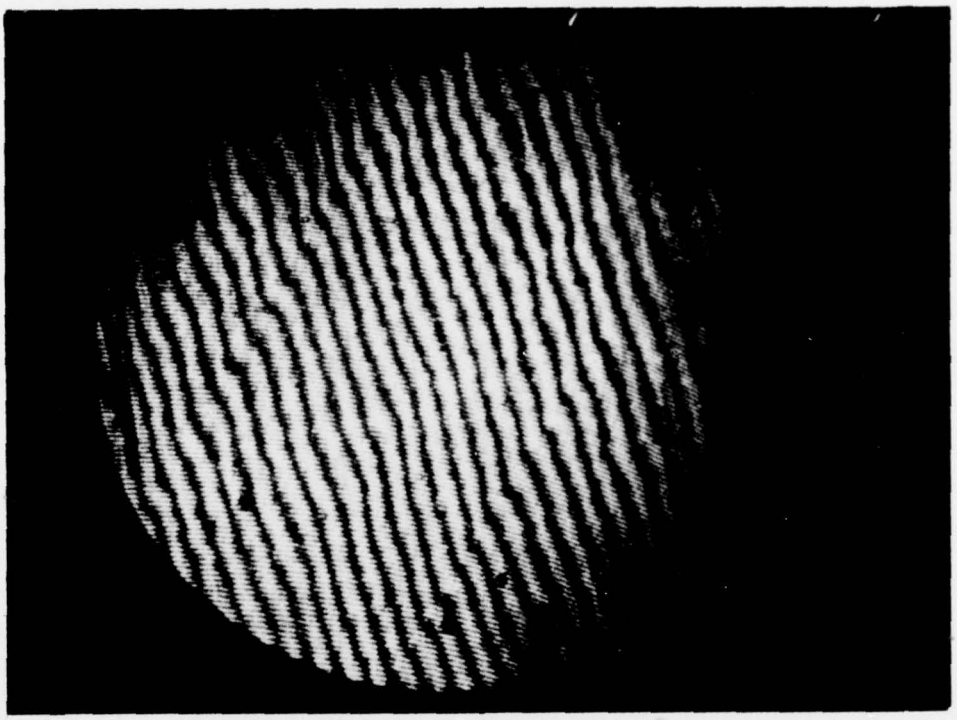

Figure 20. Interferogram of a Microflat Glass Plate.

The emulsion-stripped microflat was then replaced by a holographic element with the emulsion side facing the optical flat. Figure 21 illustrates the phase variations over the entire air/emulsion surface boundary. The central area is the clear aperture of the holographic element. The outer area is not part of the hologram. By using the same experimental arrangement, the holographic element was re-oriented with the glass side facing the optical flat. The third interferogram (figure 22) shows the phase variations over the entire air/glass boundary. Note the slightly astigmatic fringes in figure 21 as compared to the spherical fringes in figure 22. Subsequent removal and replacement of the holographic element in its holder yielded similar results. Since the holographic element is held in place by its own weight, the interferogram differences between figures 21 and 22 are evidently due to the respective surface contours. Figure 23 shows the effective wedge angle and phase variations in the emulsion-coated microflat on which the hologram is recorded. Note that in the central area that contains the hologram the wedge angle is less but the phase variations are greater than in the nonholographic (outer) area. A combination of the effects shown in figures 21 and 22 have probably contributed to the results in figure 23.

Determining the path deviation of the holographic optical element required changing the optical test system to include a second He–Ne laser positioned outside the interferometer (figure 24). This was necessary to obtain coincidence between the optical axes of the holographic optical element and the interferometer.

The alignment procedure began with the holographic element positioned normal to the interferometer's optical axis. The optical flat was replaced by a 100-millimeter-diameter f/3.3 lens (path deviation $\leq \lambda/20$) and aligned to the optical axis. The holographic element was then translated in Z until the first-order diffracted beam of light was in approximate collimation. A 50/50 beamsplitter was then positioned to reflect the collimated beam back through the interferometer. Many iterations between Z translation and X,Y rotation were necessary to obtain interference fringes over the maximum available field of view (i.e. the ratio of f-numbers 3.3/4.3, multiplied by the clear aperture, 100 millimeters). As a final alignment check, an external laser was placed 2 meters from the holographic element and adjusted until all surface back-reflections were coincident upon the exit pupil of the laser (figure 24). Any reflections not coincident on the pupil indicated a need for additional longitudinal and rotational alignment adjustments.

After alignment was achieved, the holographic element was deliberately translated 15 micrometers in X and rotated 20 arc seconds about Y to generate parallel fringes (figure 25). In double-pass view, the path deviation of this holographic element

Figure 21. Interferogram of the Air/Emulsion Surface of a Holographic Optical Element.

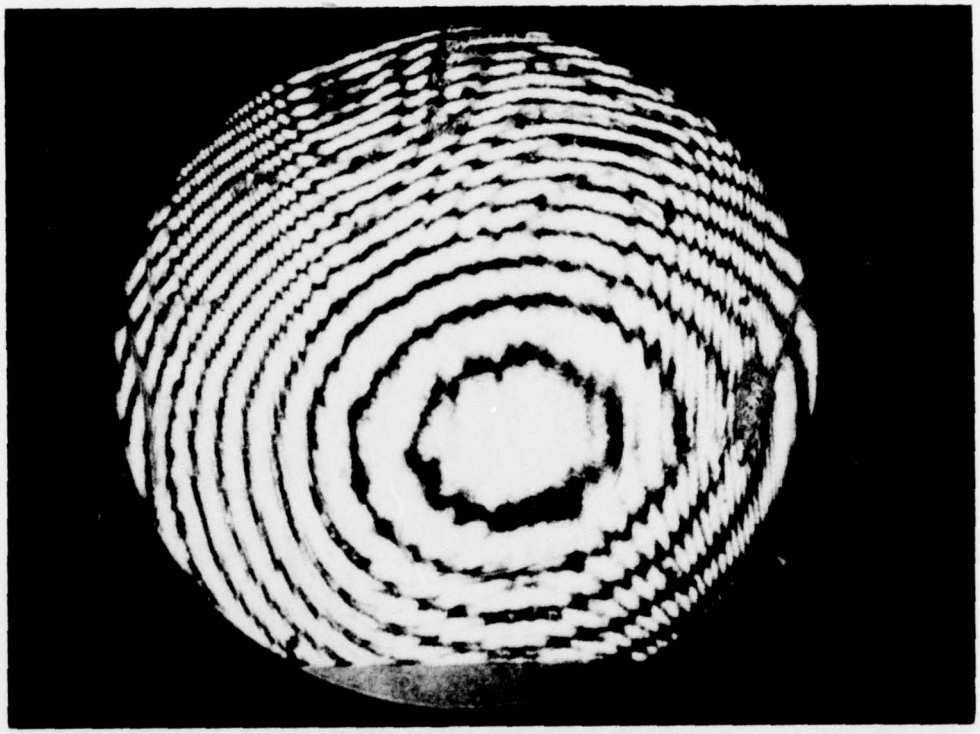

Figure 22. Interferogram of the Air/Glass Surface of a Holographic Optical Element.

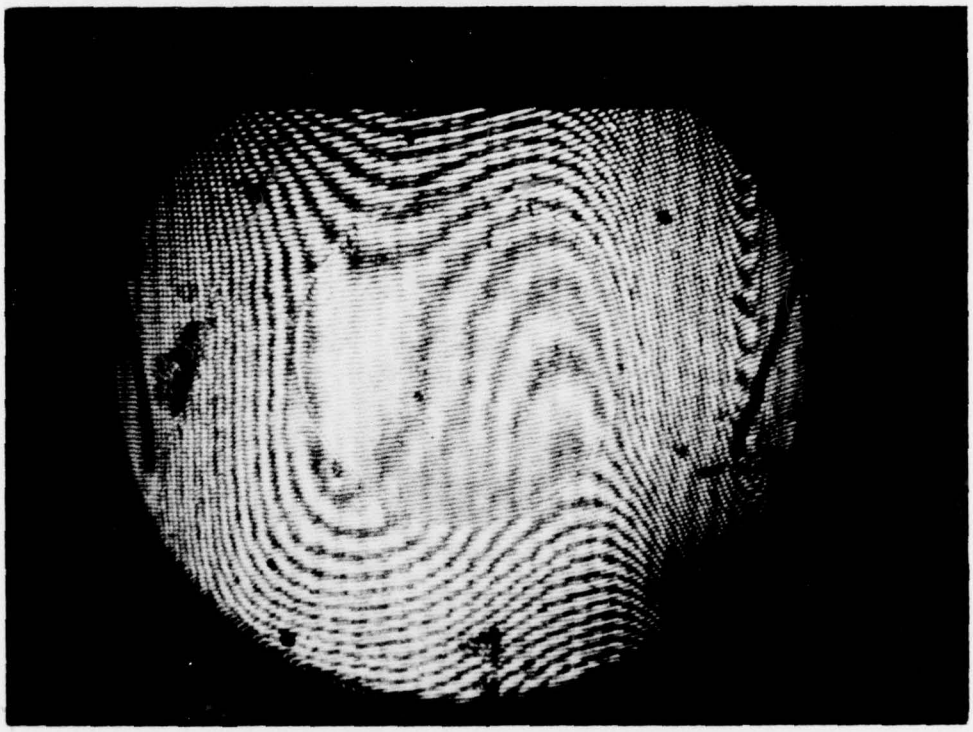

Figure 23. Interferogram of the Emulsion and Glass Medium of a Holographic Optical Element.

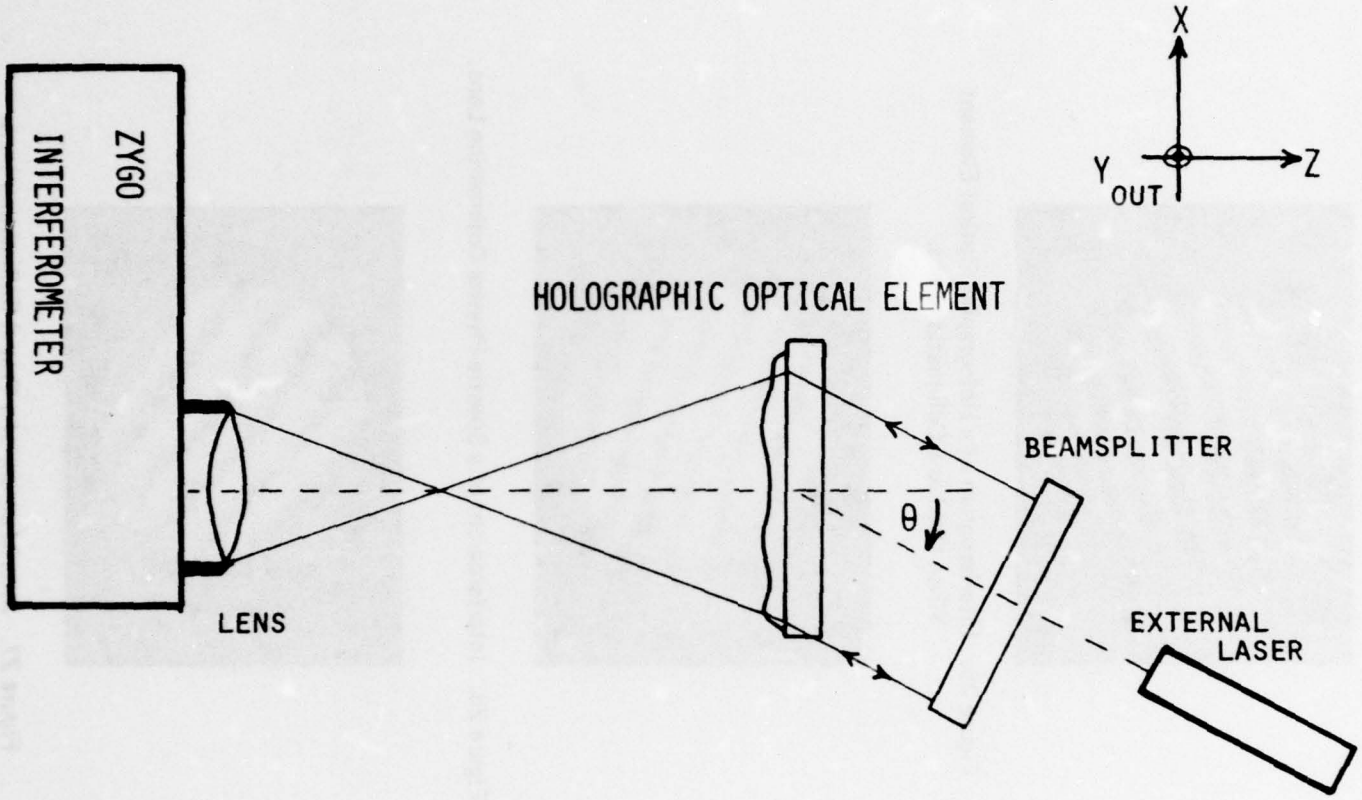

Figure 24. Experimental Arrangement Used to Produce Figure 25.

Figure 25. Interferogram of a Holographic Optical Element When Used as a Collimating Lens.

Figure 26. Interferogram of a Spectra-Physics Collimating Lens.

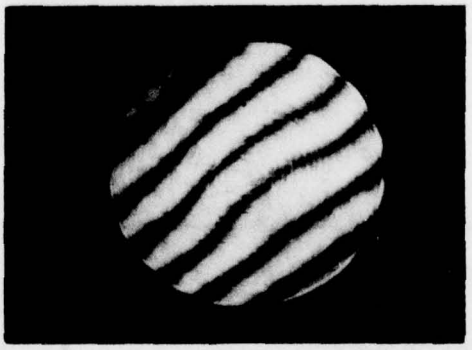

Figure 27. Interferogram of a Tropel Collimating Lens.

is $\leq \lambda/4$. Additional measurements produced a path deviation $\leq \lambda/4$ for three out of six holographic elements. Variations in results may have originated from differences in exposure, from K-ratio and processing, or simply from 2 years of aging. The problem is difficult to resolve at this time.

For the purpose of comparison, two high quality 200-millimeter f/4 collimating lenses, Model 336, Spectra-Physics, Inc. and Model 280-50, Tropel, Inc. were tested. A conventional optical setup was used in which the holographic element was replaced by a collimating lens, and the beamsplitter positioned normal to the optical axis (figure 24). The interferogram in figure 26 was generated by the Spectra-Physics lens. The Tropel lens tested out similarly (figure 27). Both lenses showed a path deviation $\leq \lambda/8$ in doublepass.

CONCLUSIONS

Theoretical considerations required by low Q-factor holograms were discussed and incorporated in the physical construction of six holographic optical elements. The optimum reference-to-subject-intensity (K) ratio ranged from 1.50 to 1.00. Optical path deviations, in three out of six HOE, were measured at $\lambda/4$, as compared measurements of $\lambda/8$ produced from two high quality collimating lenses. Although smaller path deviations were desirable, the results from the holographic optical element were quite good considering the interferometric quality of the microflat glass plate and the statistically small samples tested. At some later date, additional analysis may be achieved by using a holographic ray-trace computer program.[19]

The technical benefits of the low Q-factor hologram were evident in the experimental results: (1) efficiency measurements of 50 percent for the first-diffraction order compared quite well with the 60 percent theoretical upper limit,[20] and (2) a reconstruction sensitivity of 14 degrees of latitude enabled easier alignment with the interferometer.

Holographic optical elements may be incorporated in most optical systems using laser light. Numerous examples include: (1) a scanner lens for beam deflection, (2) an optical Fourier-transforming lens for spatially filtering images, (3) a collimator lens for distance ranging equipment, (4) an imaging lens for holographic storage and display systems, etc.

---

[19] E.A. Magerum, *Holographic Ray Tracing and Spot Diagrams*, U.S. Army Engineer Topographic Laboratories, Fort Belvoir, Va., ETL-0052, August 1975, NTIS; AD-A027 043.

[20] W.R. Klein, "Theoretical Efficiency of Bragg Devices," *Proceedings of the IEEE*, Vol. 54, 1966, P. 803.

Major advantages in the application of holographic optical elements lie in (1) their low cost, approximately $20.00 (U.S.) production cost for a 100-millimeter-diameter, f/1.2 lens, and (2) their customizing capability, diameter and f-number design is limited only to the size of photosensitive material and optical components used in the HOE construction.